Proteomic analysis revealed the function of PoElp3 in development, pathogenicity, and autophagy through the tRNA-mediated translation efficiency in the rice blast fungus

Yuanhao Liu[1,†], Ting Sun[1,†], Yuyong Li[1,†], Jianqiang Huang[2,†], Xianjun Wang[2], Huimin Bai[2], Jiayi Hu[2], Zifan Zhang[1], Shuai Wang[1], Dongmei Zhang[2], Xiuxiu Li[2], Zonghua Wang[4,*], Huakun Zheng[1,*], Guifang Lin[3,*]

[1] Fujian Universities Key Laboratory for Plant Microbe Interaction, College of Life Sciences, Fujian Agriculture and Forestry University, Fuzhou 350002, China.

[2] State Key Laboratory of Ecological Pest Control for Fujian and Taiwan Crops, College of Plant Protection, Fujian Agriculture and Forestry University, Fuzhou 350002, China.

[3] Basic Forestry and Proteomics Research Center, Fujian Agriculture and Forestry University, Fuzhou, 350002, China.

[4] Fuzhou Institute of Oceanography, Minjiang University, Fuzhou 350108, China.

* Correspondence: glin2150@163.com (G.L.); huakunz2017@fafu.edu.cn (H.Z.); wangzh@fafu.edu.cn (Z.W.).

† These authors contributed equally to this work.

Abstract

The Elongator complex is conserved in a wide range of species and plays crucial roles in diverse cellular processes. We have previously shown that the Elongator protein PoELp3 was involved in the asexual development, pathogenicity, and autophagy of the rice blast fungus. In this study, we further revealed that PoElp3 functions via tRNA-mediated protein integrity. Phenotypic analyses revealed that overexpression of two of the tRNAs, tK(UUU) and tQ(UUG) could rescue the defects in Δ*Poelp3* strain. TMT-based proteomic and transcriptional analyses demonstrated that 386 proteins were down-regulated in Δ*Poelp3* strain compared with wild type strain Guy11, in a transcription-independent manner. Codon usage assays revealed an enrichment of Glutamine CAA-biased mRNA in the 386 proteins compared with the 70-15 genome. In addition to those reported previously, we also found that PoErp9, a sphingolipid C9-methyltransferase, was down-regulated in the Δ*Poelp3* strain. Through an *ILV2*-specific integration of *PoERP9-GFP* into the wild type and Δ*Poelp3* strain, we were able to show that PoErp9 was positively regulated by PoElp3 translationally but not transcriptionally. Functional analyses revealed that PoErp9 was involved in the fungal growth, conidial development, pathogenicity, and TOR-related autophagy homeostasis in *P. oryzae*. Taken together, our results suggested that PoElp3 acts through the tRNA-mediated translational efficiency to regulate asexual development, pathogenicity, and autophagy in the rice blast fungus.

Key words: Elongator, tRNA, proteomics, transcription, translational efficiency, rice blast fungus

1. Introduction

Transfer RNAs (tRNAs) are central players in protein biosynthesis that decipher the genetic code of mRNA and add appropriate amino acids into the growing amino acid chain (Holley *et al.* 1965; Ma *et al.* 2021). The simple primary sequence of tRNAs determines that it could fold into a diverse structure in addition to the one with biological function. Therefore, the posttranscriptional modifications of tRNA are essential for the maturing, folding, degradation, and decoding efficiency (Sokołowski *et al.* 2018). The 5-methoxycarbonylmethyl- 2-thiouridine (mcm^5s^2) modification of tRNA at U_{34} is one of the best-studied modifications and is conserved in many species (Leidel *et al.* 2009; Sokołowski *et al.* 2018). The mcm^5s^2-modified tRNAs decipher the NAA type codons and wobble onto NAG. For example, the lysine, glutamine, and glutamic acid are encoded by either AAA, CAA, and GAA, or AAG, CAG, and GAG, respective. And a single eukaryotic tRNA ($tRNA^{Lys}{}_{UUU}$ (tK^{UUU}), $tRNA^{Glu}{}_{UUC}$ (tE^{UUC}), or $tRNA^{Gln}{}_{UUG}$ (tQ^{UUG})) with a U at position 34 can recognize both the NAA and NAG (wobble) codons (Dewez *et al.* 2008; Goffena *et al.* 2018). The Elongator complex is involved in the first step of mcm^5s^2 modification by transferring a carboxymethyl group to U_{34} at the C_5 position to form the 5-carboxymethyluridine (cm^5U) precursor (Selvadurai *et al.* 2014). Although Elongator complex was found to modify 11 U_{34}-carrying tRNA species, only tK^{UUU}, tE^{UUC}, and tQ^{UUG} were subsequently thiolated (S2) (Johansson *et al.* 2008).

Elp3 is the catalytic subunit of the Elongator complex, which was originally identified in *Saccharomyces cerevisiae* as a component of elongating RNA polymerase II (RNAPII) holoenzyme (Otero *et al.* 1999). Elp3 contains a Gcn5-related N-terminal histone acetyltransferase (HAT) domain (Winkler *et al.* 2002), which was reported to have the acetyltransferase activity on histone protein and other proteins (Creppe *et al.* 2009; Miśkiewicz *et al.* 2011; Laguesse *et al.* 2017; Lin *et al.* 2019; Planelles-Herrero *et al.* 2022). However, the effect of Elp3 on histone acetylation could be altered in different organisms,

86 in suggestive of diverse regulatory mechanisms in different backgrounds. For
87 example, the H3K14ac level was significantly reduced in *S. cerevisiae*
88 (Wittschieben *et al.* 2000), *Fusarium graminearum* (Lee *et al.* 2014) and
89 *Beauveria bassiana* (Cai *et al.* 2022), but not in *Aspergillus fumigatus* (Zhang
90 *et al.* 2022) and *Pyricularia oryzae* (Zhang *et al.* 2021). Elp3 also possesses a
91 radical S-adenosylmethionine (SAM) domain, which is responsible for the
92 modification of wobble uridine residues in eukaryotic tRNA (Dauden *et al.* 2019;
93 Lin *et al.* 2019; Abbassi *et al.* 2020). Increasing evidence demonstrated that
94 overexpression of corresponding hypomodified tRNA could rescue the defects
95 caused by Elongator complex-associated s^2U_{34} deficiency in many organisms,
96 such as *S. cerevisiae* (Esberg *et al.* 2006; Nedialkova and Leidel 2015;
97 Tükenmez *et al.* 2015; Jaciuk *et al.* 2023), *Caenorhabditis elegans*
98 (Nedialkova and Leidel 2015), and *Aspergillus fumigatus* (Zhang *et al.* 2022).
99 In line with this, studies in different species demonstrated that both the SAM
100 and KAT domains are required for the modification of tRNA by Elp3 proteins
101 (Selvadurai *et al.* 2014; Zhang *et al.* 2022). These results further support a key
102 role of Elongator complex in maintaining the wobbling function of tRNA.
103 In *P. oryzae* (syn. *Magnaporthe orzyae*), causal agent of the destructive
104 blast disease, autophagy is crucial for diverse developmental processes,
105 particularly, the appressorial development (Liu *et al.* 2007; Wilson and Talbot
106 2009; He *et al.* 2018; Sun *et al.* 2018; Yin *et al.* 2019). We had previously
107 shown that the Elp3 homolog was required for the development and
108 pathogenicity in the rice blast fungus *P. oryzae*, probably by maintaining the
109 autophagy homeostasis (Zhang *et al.* 2021). In this study, we aim to
110 investigate whether PoElp3 is involved in the wobbling function of tRNA and
111 subsequently the proteomic integrity.
112
113 **2. Materials and methods**
114 **2.1. Manipulation of fungal strains**
115 The fungal strains were cultivated as described previously (Anjago *et al.* 2022).

116 In brief, all strains were grown at 28 ºC on complete medium (CM, containing
117 yeast extract 0.6%, casamino acid 0.6%, sucrose 1%, agar 2%). For
118 rapamycin inhibition assay, the strains were grown at 28 ºC on MM medium
119 supplemented with or without 1 μg/mL rapamycin (He *et al.* 2018). All the
120 assays were repeated three times with at least three replicates in each
121 biological repeat.

122 **2.2. Spray inoculation assay**

123 The spray inoculation assays were performed as previously described with
124 minor modification (Zhang *et al.* 2021). Conidial suspensions (5×10^4
125 conidia/mL in 0.025% Tween-20 solution) of each strain were used for spray
126 inoculation assay on 14-day-old TP309 (Fig. 1) or NPB (Fig. 6) rice seedlings.
127 The challenged rice seedlings were then cultivated under the conditions
128 described previously (Giraldo *et al.* 2013). The symptoms were recorded and
129 scored as previously described (Valent *et al.* 1991).

130 **2.3. Construction of tRNA overexpression strains**

131 For the identification of $tRNA^{Lys}{}_{UUU}$ (tK^{UUU}) and $tRNA^{Gln}{}_{UUG}$ (tQ^{UUG}), we search
132 the rice blast genome for the homologs of SPBTRNALYS.06 and
133 SPBTRNAGLN.02, respectively, from *Schizosaccharomyces pombe*
134 (Appendix A). The identified coding sequences of each tRNA were amplified
135 using the primers listed in Appendix B and inserted into the *Xho*I and *Hind*III
136 sites of pKNT-RP27, which was then introduced into the Δ*Poelp3* strain
137 through the PEG3350-meidiated protoplast transformation (Sweigard *et al.*
138 1998). The resulting transformants were selected on TB3 medium with 600
139 μg/mL G418 and further tested through PCR-based genotyping.

140 **2.4. Proteomics analysis**

141 The proteomic analysis was performed as previously described with some
142 modifications (Zhang *et al.* 2022). Tandem Mass Tags (TMT)-based
143 proteomics analysis was conducted by Jingjie PTM Bio (Hangzhou, China). 50
144 μg total protein of each sample was digested with trypsin for TMT labeling and
145 fraction. The LC-MS/MS analysis was performed using an Orbitrap Exploris™

146 480 mass spectrometer (Thermo Scientific™, USA). The MS raw data were
147 processed with Proteome Discoverer (v2.4.1.15) and searched against 70-15
148 reference genome (Dean *et al.* 2005).

149 **2.5. RNA-sequencing and data analysis**

150 The RNA-sequencing and data analysis were performed as described
151 previously (Xie *et al.* 2023). The total RNA of each sample was used for the
152 construction of the RNA-seq library as described previously (Zhong *et al.*
153 2019). The libraries were sequenced using the Illumina NovaSeq 6000 system.
154 Quality assessment of raw reads (RNA-seq) was conducted using FASTQC
155 v0.11.3 (www.bioinformatics. babraham.ac.uk/bugzilla/). Adapters were
156 removed from the raw reads using Trim_galore v3.1
157 (https://github.com/FelixKrueger/TrimGalore/). Then, the RNA-seq reads were
158 aligned to 70-15 reference genome (Dean *et al.* 2005) using RSEM v1.3.3 (Li
159 and Dewey 2011). The quantification of expression counts were conducted
160 with transcript per million (TPM).

161 **2.6 Generation of the *ILV2*-specific *PoERP9-GFP* integration strains**

162 The construction of the *ILV2*-specific *PoERP9-GFP* integration vector and the
163 generation of *ILV2*-specific *PoERP9-GFP* integration strains was performed as
164 described previously (Yang and Naqvi 2014). The native promoter and coding
165 sequence were amplified respective using the primers listed in appendix B and
166 inserted into *pKNT-GFP*. The resultant construct
167 *pKNT-PoERP9p-PoERP9-GFP* was used as the template for the amplification
168 of *PoERP9p-PoERP9-GFP* fusion, which was them integrated into
169 pFGL1010-GFP. The resultant construct pFGL1010-PoERP9p-PoERP9-GFP
170 was transformed into the *Agrobacterium tumefaciens* AGL1 strain via
171 electroporation. The *A. tumefaciens*-mediated transformation (ATMT) of rice
172 blast fungus was performed as described previously (Yang and Naqvi 2014).

173 **2.7. Targeted gene deletion and complementation of *PoERP9***

174 Strategy for the targeted gene deletion of *PoERP9* and the construction of
175 complemented strain (Δ*Poerp9c*) was performed as described previously

176 (Zhang *et al.* 2021). In brief, the upstream fragment (A) and downstream
177 fragment (B) were amplified using *ERP9AF* & *ERP9AR*, and *ERP9BF* &
178 *ERP9BR* (Appendix B), which were then fused with the 5´-terminal (HY) and
179 3´-terminal (YG) of hygromycin B phosphotransferase cassette (HPH),
180 respectively, to form the 'A-H' and 'H-B' fusion constructs (Appendix C),
181 respectively. The 'A-H' and 'H-B' fusions were introduced into the *Ku80*
182 protoplasts using the PEG-mediated transformation method as described
183 previously (Kershaw and Talbot 2009). PCR-based genotyping of the deletion
184 strain was performed using the primer pairs *ERP9tF* & *ERP9tR*, and
185 *ERP9UAF* & *H853* (Appendix B). Southern blot assay was performed for to
186 validate the mutant candidates.

187 For complementation of Δ*Poerp9* strain, genomic DNA fragment containing
188 the native promoter, ORF region, and 3´-untranslated region (UTR) of *PoERP9*
189 was amplified from the Guy11 genomic DNA using primers *ERP9comF* and
190 *ERP9comR* (Appendix B) and inserted into *pKNTG* vector carrying the
191 neomycin resistance cassette. The resulting construct was transformed into
192 the Δ*Poerp9* protoplasts as described above. The neomycin resistant colonies
193 were evaluated through PCR-based identification using the primer pairs
194 *ERP9tF* & *ERP9tR*.

195 **2.8. Southern hybridization assay**

196 10 μg genomic DNA isolated from the indicated strains was digested with *Kpn* I
197 for the validation of Δ*Poerp9* and *Sac* I for the identification of *ILV2*-specific
198 integration of *PoERP9-GFP*. The digested products were electrophoresed in 1%
199 (w/v) agarose gel and then transferred onto positively charged Nylon
200 membranes (Roche, Germany). For both assays, the 'A' fragment amplified
201 from the Guy11 genomic DNA using primer pairs *ERP9AF*&*ERP9AR* was used
202 as probe. Probe labeling, hybridization, and detection were performed using
203 DIG High Prime DNA Labeling and Detection Starter Kit I (Roche) according to
204 the instruction manual.

205 **2.9. Western hybridization assay**

206 The Western blotting assays were performed as described previously (Zhang
207 *et al.* 2021). The mycelial pellets were ground into fine powder in liquid
208 nitrogen and transferred into 1 mL extraction buffer (10 mmol L^{-1} Tris-HCl pH
209 7.5, 150 mmol L^{-1} NaCl, 0.5 mmol L^{-1} EDTA, 0.5% NP-40, 2 mmol L^{-1} PMSF).
210 After the resuspension and centrifuge, SDS-PAGE was performed to resolve
211 the proteins. For western blot assays, the resolved protein samples were
212 transferred onto a PVDF membrane (Merck Millipore Ltd., USA) through a
213 Bio-Rad electrophoretic blotting apparatus. The detection of PoErp9-GFP
214 fusion and Actin was performed as described previously with minor revision
215 (Zhang *et al.* 2021). The whole-cell extract detection assays were carried out
216 with an anti-GFP antibody (Abmart, China), anti-Actin antibody (Huadingbio,
217 China), and an anti-mouse secondary antibody (Abmart, China). After the
218 incubation with the antibodies, the Western Bright ECL HRP substrate
219 (Advansta, Menlo Park, USA) was used to detect the chemiluminescent
220 signals.

221 **2.10. Quantitative real-time PCR (qRT-PCR)**

222 First strand cDNA was generated from 1 μg of total RNA using the Prime Script
223 RT Reagent Kit with gDNA Eraser (TaKaRa, Dalian, China). Real-time PCR
224 was performed by using an SYBR Green PCR Master Mix (TaKaRa, Dalian,
225 China) and the primers listed in Appendix B.

226 **2.11. Live-cell imaging assay**

227 To image invasive hyphae, spore solution (10^5 sporse mL^{-1} in ddH2O) of each
228 strain was inoculated into the leaf sheath of susceptible rice cultivar CO39. For
229 rapamycin inhibition assay, conidial suspension with or without 1 μg mL^{-1}
230 rapamycin was inoculated onto the leaf sheath of CO39. The invasive hyphae
231 were recorded at 24 hpi using Nikon A1R laser scanning confocal microscope
232 system (Nikon, Japan) as previously reported (Zheng *et al.* 2017).

233 **2.12. Statistical analysis**

234 Statistical analysis was conducted by R packages in the R studio (Version
235 1.4.1106) environment (Xie *et al.* 2023).

236 **3. Results**

237 **3.1. Overexpression of tRNA could rescue the defects in Δ*Poelp3* strain**

238 To test whether the overexpression of tRNA could complement the defects
239 showed in Δ*Poelp3* strain, we search in the rice blast fungal genome for genes
240 encoding tK^{UUU} and tQ^{UUG}, the two tRNA that could rescue the transcription
241 and histone acetylation defects, as well as other phenotypes caused by the
242 absence of Elongator when overexpressed (Esberg *et al.* 2006). We found that
243 both tRNAs have two coding genes, with tK^{UUU}-4 and tK^{UUU}-6 localized at chr4
244 and chr6, tQ^{UUG}-2 and tQ^{UUG}-4 localized at chr2 and chr4, respectively. The
245 coding sequence of the two copies of each tRNAs was highly conserved, while
246 the franking sequences were highly polymorphic (Appendix A). The four tRNA
247 coding genes were fused with the ribosomal protein promoter (*RP27p*) and
248 introduced into the Δ*Poelp3* strain, respectively. At 7 days post inoculation, the
249 diameter of transfromants carrying the *RP27p* :: tK^{UUU} (herein after referred to
250 as '*tK(UUU)*') or *RP27p* :: tQ^{UUG} (herein after referred to as '*tQ(UUG)*') was
251 about 95%-100% of that of wild type, while the diameter of Δ*Poelp3* strain was
252 about 85% of that of the wild type (Fig. 1-A and B). Upon the treatment of
253 rapamycin, inhibitor of the Target-of-Rapamycin (TOR) signaling pathway, the
254 inhibition rate of fungal growth in the tK^{UUU} and tQ^{UUG} strains was reduced
255 compared to Δ*Poelp3* strain, but was still larger than that of Guy11 (Fig. 1-A
256 and C). Spray inoculation results showed that expression of tK^{UUU} and tQ^{UUG}
257 could also partially rescue the defects in pathogenicity caused by the absence
258 of *PoELP3* (Fig. 1-D and E). These results suggested that the defects caused
259 by the deletion of *PoELP3* were at least partially caused by the inefficiency in
260 protein biosynthesis.

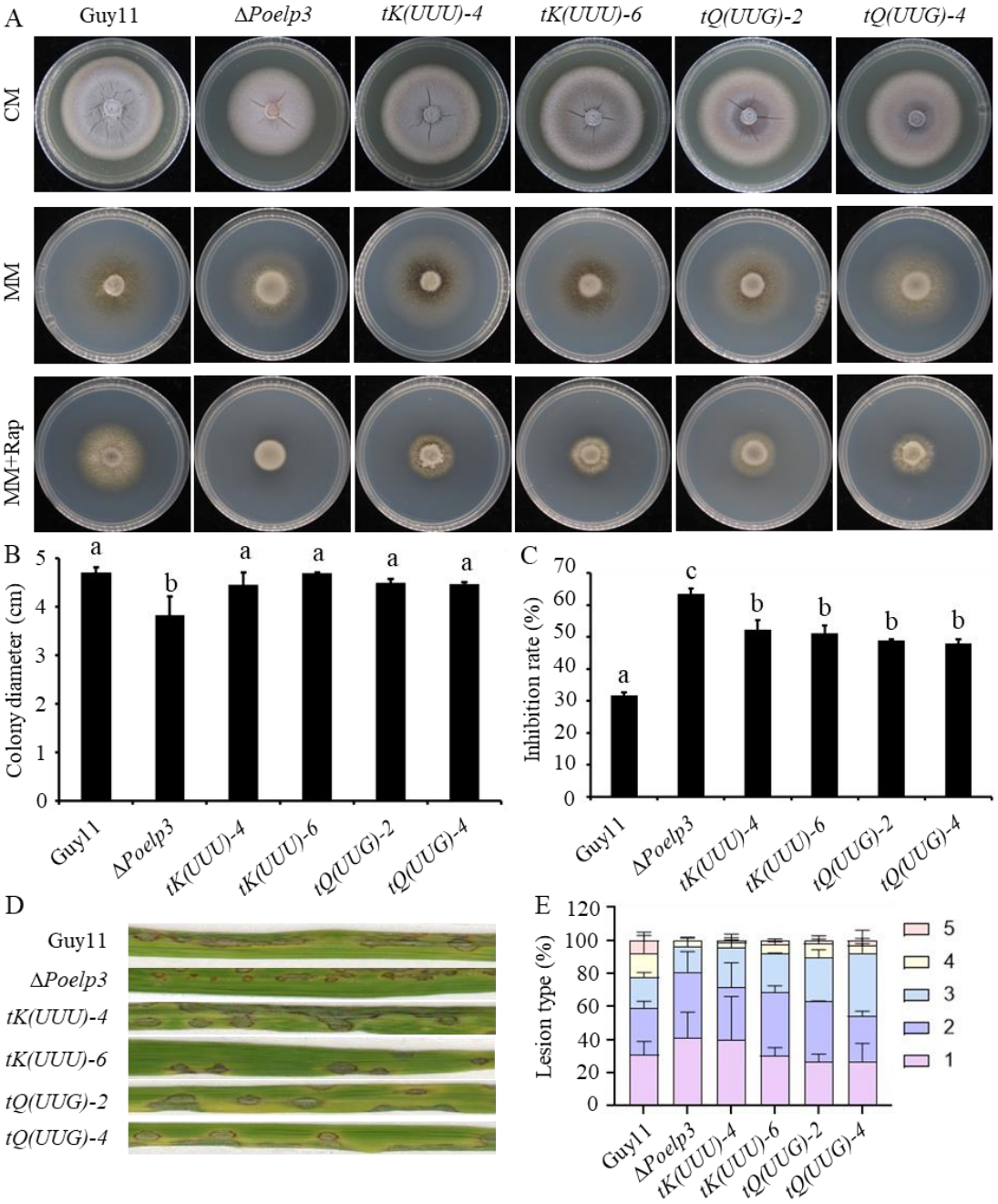

Fig. 1 Overexpression of *tK*(*UUU*) or *tQ*(*UUG*) could partially rescue the defects in Δ*Poelp3* strain. A, the indicated strains grown on CM, MM and MM supplemented with 1 μg/uL rapamycin (MM+Rap). B, colony diameter of indicated strains grown on CM. C, the inhibition rate of indicated strains upon the treatment of 1 μg/uL rapamycin. The letters indicate statistically significant differences ($p<0.01$). D, leaves of rice cultivar TP309 were sprayed with conidial suspensions (5×10^4conidia mL^{-1}) of strains indicated. E, quantification of different lesion types. Data were shown as the mean±SE (n=3).

270 **3.2. PoElp3 is involved in the proper expression of protein**

271 To further investigate how PoElp3 regulates fungal development, pathogenicity,
272 and autophagy by affecting protein biosynthesis efficiency, we compared the
273 protein abundance between Δ*Poelp3* strain and the Guy11 wild type strain
274 through the tandem mass tags (TMT)-based quantitative proteomic analysis.
275 Among the 5,165 proteins identified and quantified in our proteomic data, 386
276 proteins were significantly down-regulated [fold change (FC) > 1/1.3 (*p-value* <
277 0.05)], and 403 proteins were up-regulated [FC < 1.3 (*p-value* < 0.05)] (Fig. 2-A
278 and B; Appendix D and E). The volcano plot result showed that most of the
279 differentially accumulated proteins (DAPs) with a FC ranged from 1.3 to 2.0,
280 and only a few of them with a FC >2.0 (Fig. 2-B). The clustering result showed
281 that the DAPs could be divided into different groups according to their
282 differential abundance between Guy11 and Δ*Poelp3* strain (Fig. 2-C).

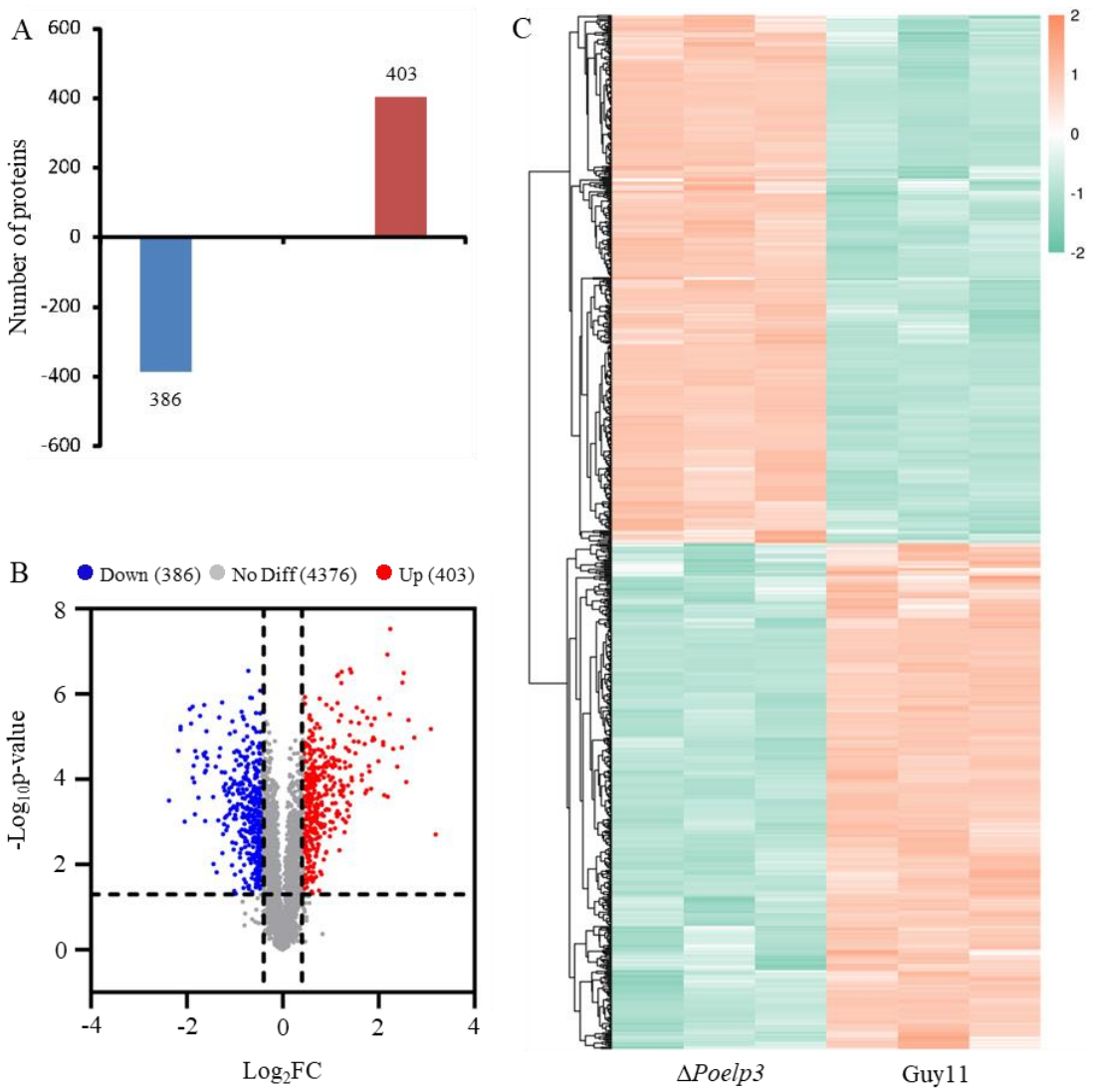

Fig. 2 The differentially accumulated proteins (DAPs) between Δ*Poelp3* and Guy11 strains. A, quantitative identification of proteins upregulated and downregulated in Δ*Poelp3* strain though TMT. B, volcano plot showing the fold change of the differentially accumulated proteins. C, cluster analysis of the DAPs.

3.3. The DAPs involved in different pathways

To perform functional classification of the DAPs, we divided the DAPs into 4 Categories: Q1 with a FC<1/1.5, Q2 with a FC between 1/1.5 to 1/1.3, Q3 with a FC between 1.3 to 1.5, and Q4 with a FC>1.5 (Fig. 3-A). KEGG enrichment results showed that the Q1 DAPs were enriched in pathways such as Glyoxylate and dicarboxylate metabolism, biosynthesis of unsaturated fatty

acids, various types of N-glcan biosynthesis, sulfur metabolism and sphingolipid metabolism. The Q2 DAPs were mainly enriched in steroid biosynthesis, tryptophan metabolism, and terpenoid backbone biosynthesis. While the Q3 and Q4 DAPs were mainly enriched in pathways such as aminoacyl-tRNA biosynthesis, biosynthesis, and metabolism of amino acids (Fig. 3-B). Protein domain enrichment showed that the Q1 DAPs were mainly enriched in pathways such as adenylysulphate kinase, fatty acid desaturase, and pyridine nucleotide-disulphide oxidoreductase. The Q2 DAPs were mainly enriched in pathways such as dynamin, flavodoxin, enoyl-(axyl carrier protein) reductase, and alpha amylase. While the Q3 and Q4 DAPs were mainly enriched in pathways such as tRNA synthetases, pyridoxamine 5'-phosphate oxidase, NADH oxidase and oxidoreductase NAD-binding domain (Fig. 3-C).

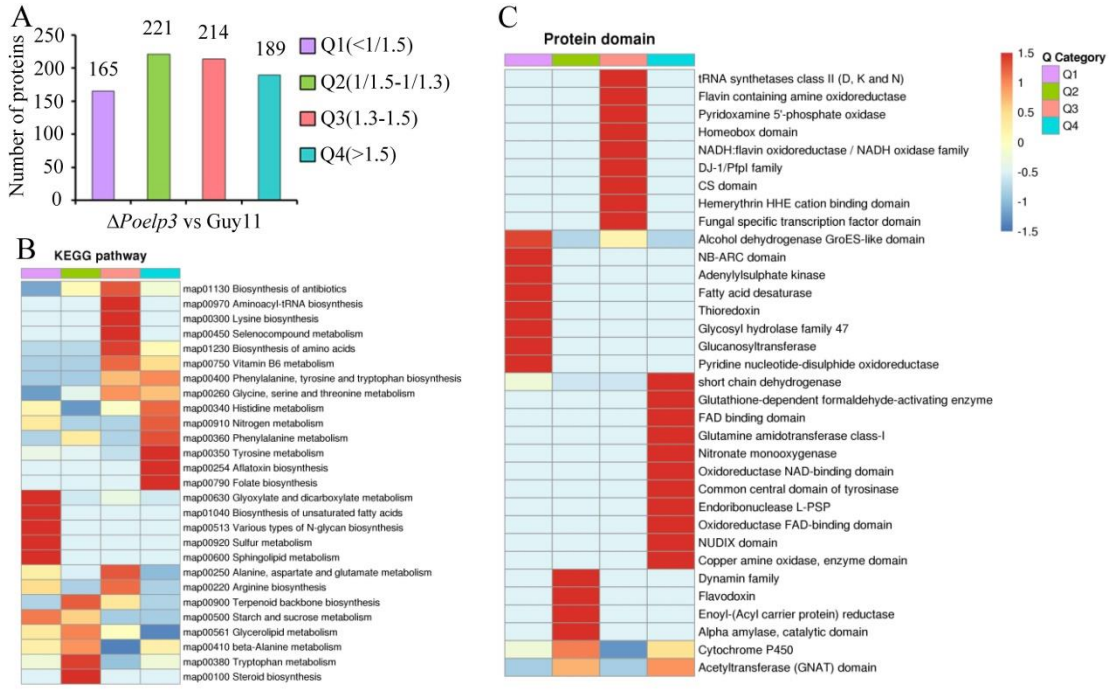

Fig. 3 Functional classification of the DAPs. A, the four Q Categories of the DAPs. B, classification of DAPs according to the KEGG pathway. C, classification of DAPs according to protein domain.

3.4. PoElp3 regulated the accumulation of proteins independent of transcription

To further assess whether the DAPs were associated with the differential transcription level of their coding genes, we performed a comparative transcriptome analysis between the wild type and Δ*Poelp3* strains. We showed that only 535 genes were down-regulated, and 1,049 genes were up-regulated in Δ*Poelp3* compared with the wild type strain Guy11 (Fig. 4-A). We further investigated the transcription level of DAPs down-regulated in Δ*Poelp3* strain, and found that, among the 386 proteins down-regulated in Δ*Poelp3* strain, only 19 and 25 of them showing either higher or lower transcription level in the mutant strain (Fig. 4-B; Appendix F). While among the 403 DAPs up-regulated in Δ*Poelp3* strain, only 22 showing lower transcription level in the mutant strain, but 138 showing higher transcription level in the mutant strain (Appendix G), which could be affected indirectly. Taken together, these results suggested that the protein level of most of the DAPs in Δ*Poelp3* strain was independent of the transcription level.

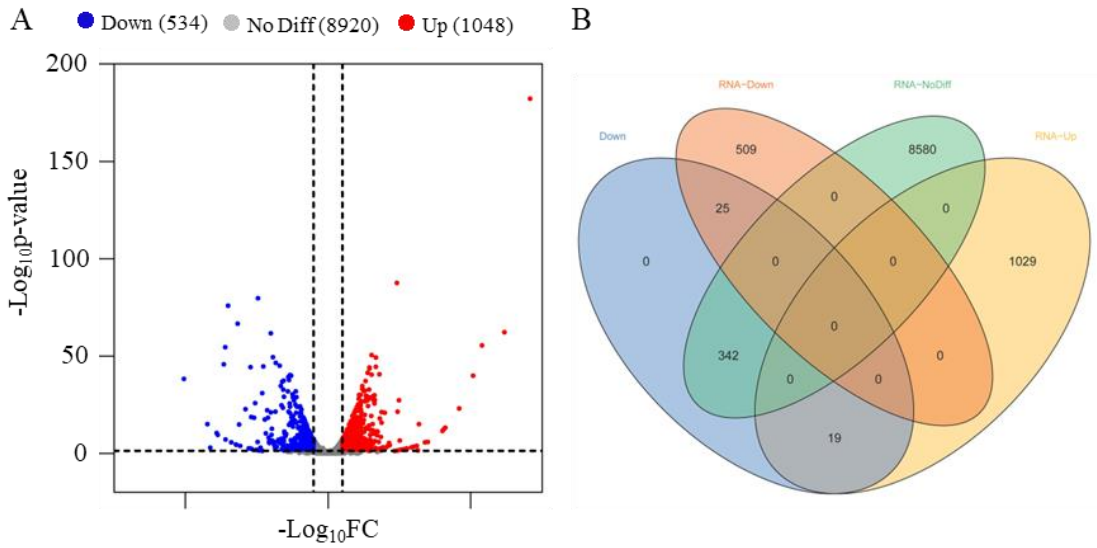

Fig. 4 Comparative transcriptional analysis between wild type and Δ*Poelp3* strains. A, differentially expressed genes between wild type and Δ*Poelp3* strains. B, comparative analysis of the transcription level of DAPs down-regulated in Δ*Poelp3* strain.

336 **3.5. Enrichment of Glutamine CAA-biased mRNA in the DAPs**
337 **down-regulated in Δ*Poelp3* strain**

338 To test whether there is a bias toward the use of NAA codons, we first
339 surveyed the coding sequence of 70-15 genome (whole genome, WG), and
340 found that 65.0%, 52.5% and 58.0% of the coding sequences showed an
341 NAA:NAG ratio > 1 for Lysine, Glutamine, and Glutamic acid, respectively
342 (Table 1). We then surveyed the coding sequence of DAPs down-regulated in
343 Δ*Poelp3* strain. Since the DAPs down-regulated in Δ*Poelp3* strain were
344 supposed to be caused by the absence of PoElp3, and are therefore referred
345 to as PoElp3 regulated protein candidates (Erps) hereafter. We found that
346 58.8.0%, 64.8% and 50.5.0% of the coding sequences showed an NAA:NAG
347 ratio > 1 for Lysine, Glutamine, and Glutamic acid, respectively (Table 1;
348 Appendix H). These results suggested an enrichment of Glutamine
349 CAA-biased mRNA in the Erps compared with 70-15 genome.

350

351 Table 1 Codon usage of lysine, glutamine and glutamic acid in the Erps.

Amino acid	Biased[a]		Non-Biased[b]		Percentage of Biased (%)	
	Erps	WG	Erps	WG	Erps	WG
Lysine	227	8,337	159	4,489	58.8	65.0
Glutamine	250	6,735	136	6,091	64.8	52.5
Glutamic acid	195	7,443	194	5,383	50.5	58.0

352 (a: NAA:NAG ratio > 1; b: NAA:NAG ratio ≤ 1.)

353

354 **3.6. The Elp3-regulated proteins involved in asexual development,**
355 **pathogenicity and autophagy**

356 To assess whether any of the DAPs down-regulated in Δ*Poelp3* strain
357 functions similarly to PoElp3, we searched in the PubMed database for
358 publications associated with the 386 DAPs and found six DAPs involved in
359 vegetative growth, conidiation, pathogenicity and/or autophagy. These DAPs

360 presented a Fold Change (FC) ranging from 0.49~0.76, and their transcription
361 level in Δ*Poelp3* strain was no less than that in Wild type strain Guy11 (Table 2
362 and Appendix F). Among them, *ERP1* encodes a core protein of ESCRT-III
363 subcomplex (Snf7) involved in asexual development, pathogenicity and
364 autophagy (Cheng *et al.* 2018). *ERP2* encoding a Rho3 homolog is involved in
365 appressorial development and pathogenicity (Zheng *et al.* 2007). *ERP3*
366 encodes an ADP-ribosylation factor 6 protein (Arf6), which is involved in
367 endocytosis and polarity during the asexual development (Zhu *et al.* 2016).
368 *ERP4* encodes a tetrahydroxynaphthalene reductase (Buf1) and is required for
369 melanin biosynthesis and full virulence (Zhu *et al.* 2021). *ERP5* encodes an
370 amidophosphoribosyltransferase (Ade4), which catalyzes the conversion of
371 5-phosphoribosyl-1-pyrophosphate into 5-phosphoribosyl-1-amine in the de
372 novo purine biosynthetic pathway and is required for conidiation and
373 pathogenicity (Aron *et al.* 2022). *ERP6* encoding a glyoxylate
374 aminotransferase 1 (Agt1) is required for mobilization and utilization of
375 triglycerides during infection (Bhadauria *et al.* 2012a; Bhadauria *et al.* 2012b).
376 Besides, we also found DAPs with their homologs in other fungal species
377 associated with development or pathogenicity. For example, the MGG_03393
378 encodes a secondary metabolism regulator (Lae1) and is involved in asexual
379 development and mycoparasitism of *Trichoderma atroviride* (Karimi Aghcheh
380 *et al.* 2013). MGG_00413T0 encoding a putative β-1,3-glucanosyltransferase
381 (Gel7) is required for the cell wall integrity under stress conditions (Zhao *et al.*
382 2014).
383
384 **TABLE 2** The *ERPs* functionally studied in *P. oryzae*

Code	Gene ID	Product	Fold Change	Function	Reference
ERP1	MGG_04174	SNF7 family protein	0.76	Vegetative growth, conidiation and pathogenicity, autophagy	(Cheng *et al.* 2018)
ERP2	MGG_10323	GTP-binding protein RHO3	0.73	Appressorial development and pathogenicity	(Zheng *et al.* 2007)
ERP3	MGG_10676	ADP-ribosylation factor 6	0.71	Vegetative growth and conidial	(Zhu *et al.*

				morphology	2016)
ERP4	MGG_02252	Tetrahydroxynaphthalene reductase MoBuf1	0.64	Conidiation, germination and pathogenicity	(Zhu *et al.* 2021)
ERP5	MGG_04618	Amidophosphoribosyltransferase	0.71	Conidiation and pathogenicity	(Aron *et al.* 2022)
ERP6	MGG_02525	Alanine-glyoxylate aminotransferase	0.49	Appressorial development	(Bhadauria *et al.* 2012a; Bhadauria *et al.* 2012b)

3.7 The accumulation of PoErp9 was positively regulated by PoElp3

We further investigated the regulation of PoErp9, a sphingolipid C9-methyltransferase (MGG_14886), by PoElp3. To exclude the discrepancy caused by different genomic environment, the *PoERP9-GFP* fusion was fused *in situ* with the sulfonylurea-resistant allele of the *ILV2* gene (Yang and Naqvi 2014) in both the wild type Guy11 and Δ*Poelp3* strain (Fig 5-A). Immunobloting results showed that the abumdance of PoErp9-GFP in the Δ*Poelp3* strain was reduced to about half of that in wild type stain (Fig. 5-B； Appendix I and J), while the transcription level of *PoERP9* was not significantly reduced in the mutant strain (Fig. 5-C). These results suggested that PoElp3 is required for the translational efficience of PoErp9 independent of transcription.

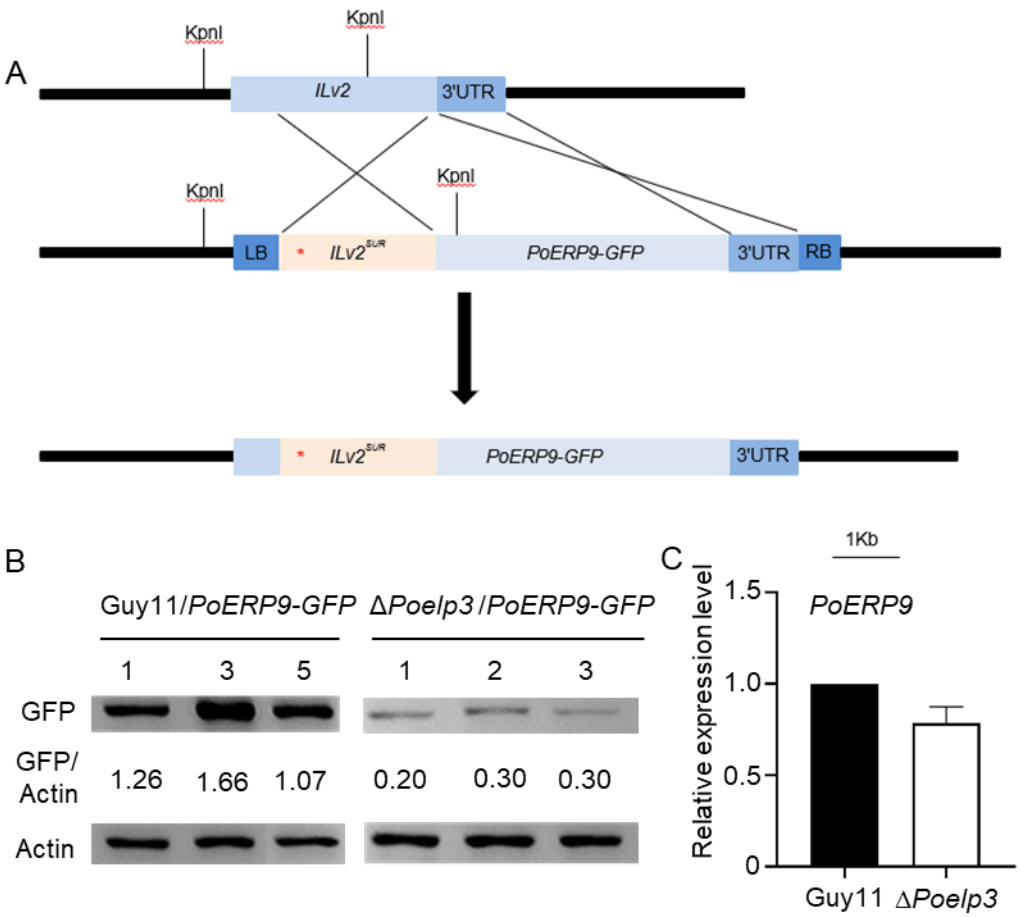

Fig. 5 The abundance of PoErp9 was reduced in the Δ*Poelp3* strain. A, strategy for the *in situ* fusion of *PoERP9-GFP* into the sulfonylurea-resistant allele of the *ILV2* gene. B, the relative abundance of PoErp9-GFP [GFP/(GFP+GFP-PoAtg8)] in wild type (Guy11) and Δ*Poelp3* strains. The numbers indicated different individual transfromants. C, relative transcription level of *PoERP9* in wild type (Guy11) and Δ*Poelp3* strains based on qRT-PCR.

3.8 PoErp9 was required for the development and pathogenicity

To assess whether PoErp9 is functionally similar to PoElp3, we generated the Δ*Poerp9* strain using the split-marker strategy (Appendix C). The Δ*Poerp9* strain displayed reduced fungal growth and conidiation by compared with that of the *Ku80* parental strain and the complemented strain (Δ*Poerp9c*) (Fig. 6-A and C). The absence of *PoERP9* also caused defect in appressorial development and pathogenicity in the blast fungus (Fig. 6-D and F). The

412 Δ*Poerp9* strain was less aggressive on the NPB leaves and generated mostly
413 level 1 and level 2 lesions, while the *Ku80* parental strain and the
414 complemented strain generated more lesions of level 3-5 (Fig. 6-E and F).
415 These results suggested that PoErp9 is required for the fungal growth,
416 appressorial development and the full virulence of the rice blast fungus.
417

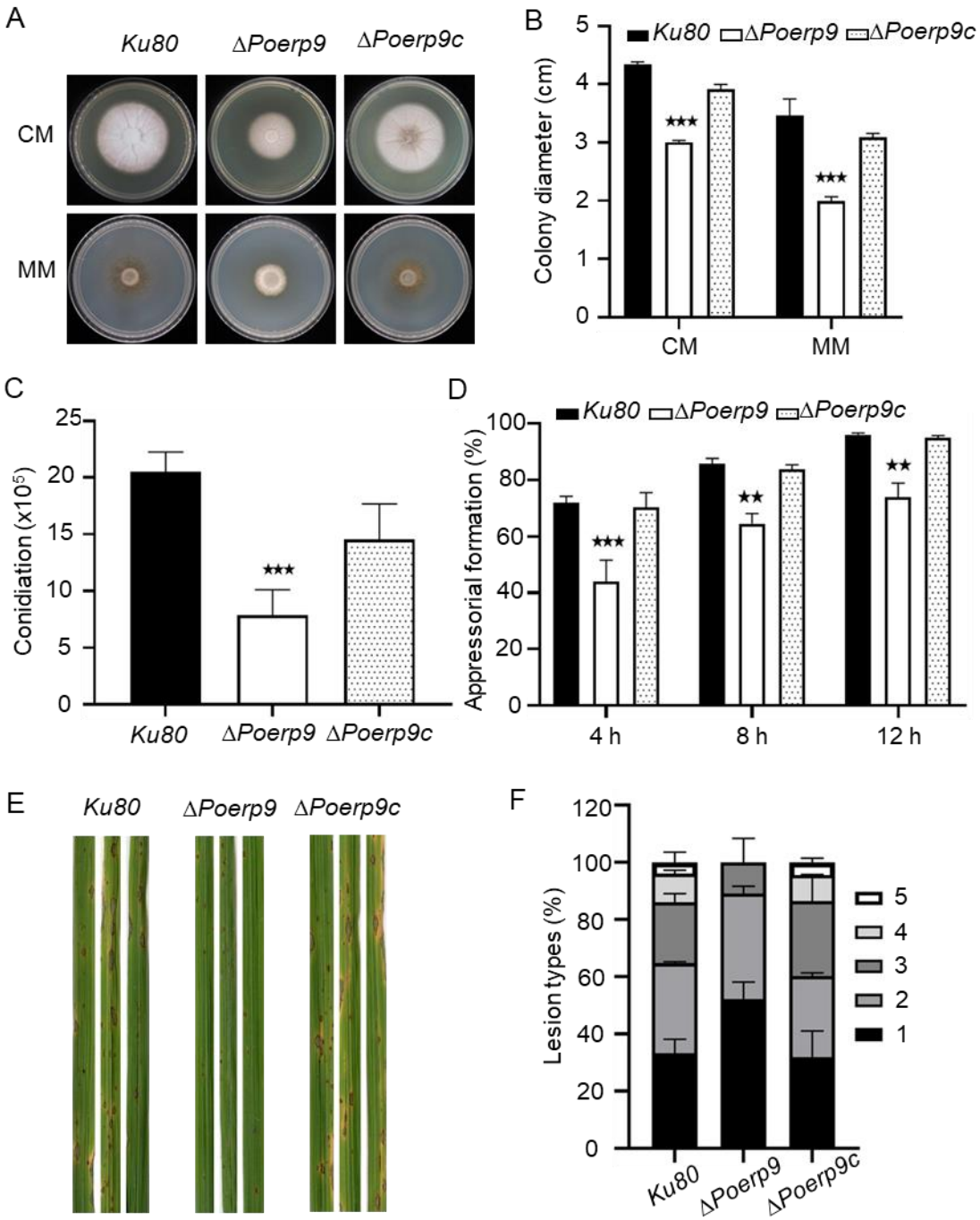

418

419 **Fig. 6** The Δ*Poerp9* strain was defective in asexual development and

420 pathogenicity. A and B, the colony morphology (A) and colony diameter (B) of
421 indicated strains on complete medium (CM) and minimal medium (MM) for 7
422 days. C, number of conidia harvested from a 7-cm rice bran plate at 3 days
423 after induction of conidiation. D, appressorial development of *Ku80*, Δ*Poerp9*
424 and Δ*Poerp9c* was observed using microscope at 4, 8 and 12 h after induction.
425 Data were shown as the mean±SE (n=3). The asterisks indicate statistically
426 significant differences (**, P<0.01; ***, P<0.001). E, leaves of rice cultivar NPB
427 were sprayed with conidial suspensions (5×10^4 conidia mL^{-1}) of strains
428 indicated. E, quantification of different lesion types. Data were shown as the
429 mean±SE (n=3).
430

431 **3.9 PoErp9 act synergistically with the TOR-signaling pathway**

432 To assess whether there is a interaction between PoErp9 and the
433 Target-of-Rapamycin (TOR) -signaling, we performed rapamycin inhibition
434 assays. Upon the treatment of rapamycin, the fungal growth of all the strains
435 grown on either CM or MM media were reduced, and Δ*Poerp9*c strain
436 displayed a higher inhibition rate by rapamycin compared with the parental
437 strain *Ku80* and the complementation strain Δ*Poerp9c* (Fig. 7-A and B). We
438 further detected the effect of rapamycin on the development of invasive
439 hyphae (IHs) at the absence of *PoERP9*. In contrast to the parental strain
440 *Ku80* and the complementation strain, the development of IH in Δ*Poerp9* strain
441 was more severely inhibited by rapamycin (Fig. 7-C), and generated fewer
442 type III and type IV IHs (Fig. 7-D). Taken together, these results suggested a
443 role of PoErp9 in the interaction with the TOR-signaling during the vegetative
444 and invasive growth of the rice blast fungus.

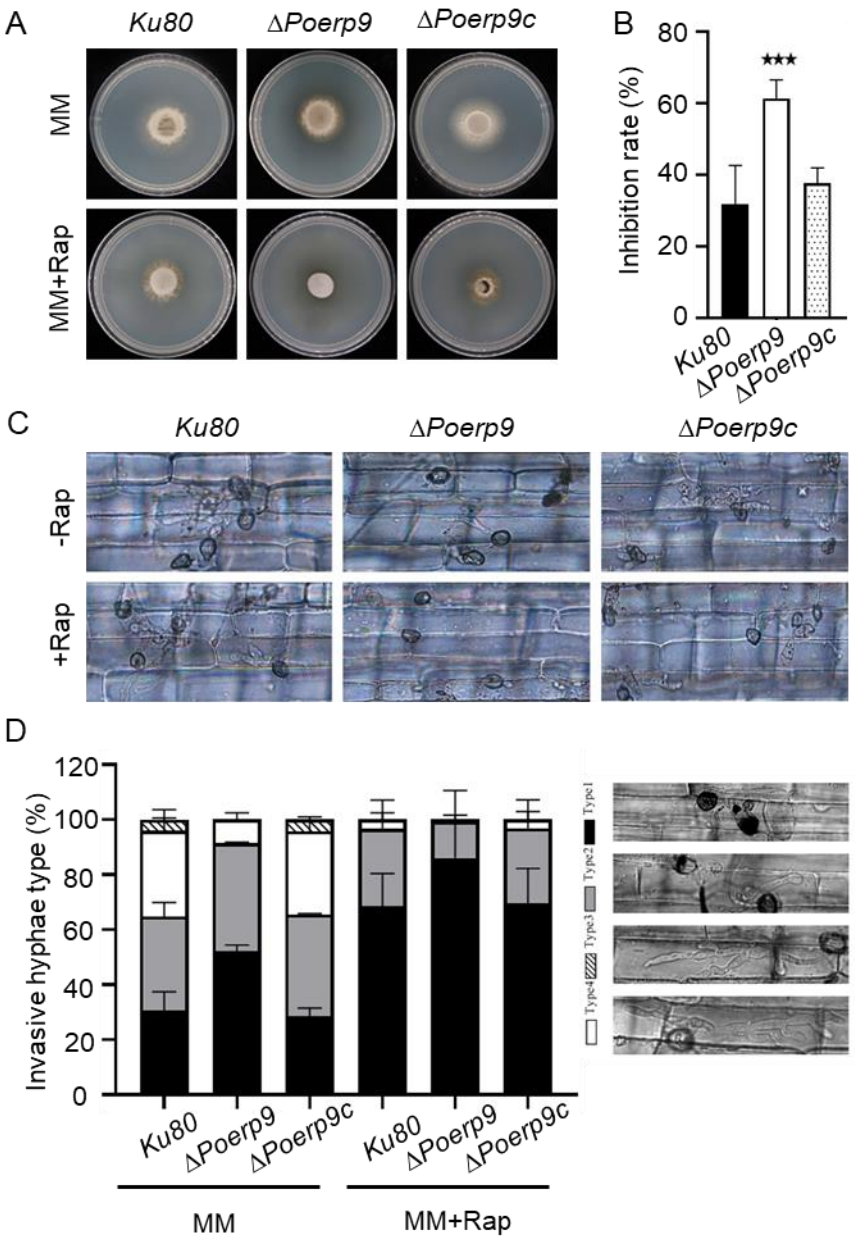

Fig. 7 PoErp9 genetically interact with TOR-signaling to regulate vegetative and invasive growth of rice blast fungus. A and C, colony morphology (A) and inhibition rate of vegetative growth of indicated strains on minimal medium (MM) treated with rapamycin (Rap). C and D, morphology (C) and types (D) of invasive hyphae in *Ku80*, Δ*Poerp9* and Δ*Poerp9*c at 24 h post-inoculation (hpi). Data were shown as the mean±SE (n=3).

4. Discussion

The Elongator complex is conserved among different species and increasing

455 evidence demonstrated that they function mainly through the modification of
456 tRNA (Bauer *et al.* 2012; Candiracci *et al.* 2019; Dauden *et al.* 2019). In
457 supporting this, overexpression of unmodified tRNA for glutamine, glutamic
458 acid and lysine was efficient to restore the defects caused by the absence of
459 Elongator in several studies (Esberg *et al.* 2006; Bauer *et al.* 2012; Zhang *et al.*
460 2022), probably by increasing the intracellular concentration of tRNAs to
461 compensate for decreased binding affinity in the Elongator mutants (Esberg *et*
462 *al.* 2006; Nedialkova and Leidel 2015; Tükenmez *et al.* 2015; Sokołowski *et al.*
463 2018). In this study, the phenotypic analysis showed that overexpression of
464 *tK*(*UUU*) or *tQ*(*UUG*) could rescue fully the defects in fungal growth, and
465 partially the defects in pathogenicity and response to rapamycin caused by the
466 deletion of *PoELP3*, which indicated that PoElp3 may act through the
467 tRNA-mediated protein integrity to regulate the fungal growth in rice blast
468 fungus (Zhang *et al.* 2021).

469 Elp3 proteins had been proved to catalyze the modification of tRNA at
470 wobbling U34 and consequently maintain the translation efficiency of proteins
471 encoded by tK(UUU), tE(UUC), or tQ(UUG) (Bauer *et al.* 2012; Goffena *et al.*
472 2018). Previous studies suggested that NAA-biased codon usage is not
473 always necessary for the Elongator regulated protein integrity via the tRNA
474 modification. For example, the biased codon usage was exhibited in yeast
475 (Bauer *et al.* 2012), but not in *A. fumigatus* (Zhang *et al.* 2022). In this study,
476 we showed that the Erps displayed an enrichment of Glutamine CAA-biased
477 mRNA, which suggested that different regulatory mechanisms might be
478 applied in the Elp3 regulated translational efficiency. Moreover, the absence of
479 NAA-biased cytoplasmic effectors on BIC as well as turnover of mRNA caused
480 by the ribosomal pausing (Li *et al.* 2023) were not observed in Δ*Poelp3*.
481 Possible explanations include that: 1) Elongator complex catalyzes the early
482 step of mcm5s2 modification at U34 of tRNA, and 2) there are complementary
483 pathways for the function of Elongator complex in the modification of U34.

484 The Elongator proteins could act by regulating the translational

485 efficiency of target with important functions. For example, in fission yeast, the
486 Elongator controls cell division by regulating the translational efficiency of the
487 Cdr2 kinase (Bauer *et al.* 2012). Our functional assessment of the Erps
488 showed that some of them were associated with asexual development, such
489 as Erp1/Snf7, Erp2/Rho3, Erp3/ArF6, Erp4/Ade4, Erp5/Buf1, Erp6/Agt1, Lae1
490 and Gel7. Recent study in *A. fumigatus* showed that defects in development
491 and pathogenicity in Δ*elp3* strain could be caused by the amino acid
492 homeostasis imbalance (Zhang *et al.* 2022). We also found that many Erps
493 were involved in the biosynthesis and metabolism of amino acids, suggesting a
494 role of PoElp3 in development and pathogenicity by modulating amino acid
495 homeostasis. Moreover, we also found Erps that may be involved in autophagy
496 through different mechanisms. For example, Erp1/Snf7 acts in vesicle
497 trafficking and autophagy (Cheng *et al.* 2018). Erp3/Arf6 is involved in
498 autophagy homeostasis through the generation of phosphatidylinositol
499 4,5-bisphosphate (PIP(2)) and induction of phospholipase D (PLD) activity
500 (Moreau *et al.* 2012). The absence of Erp4/Ade4 caused delayed glycogen
501 mobilization and reduced turgor pressure in the appressoria (Aron *et al.* 2022),
502 the representative cellular processes of autophagy during appressorial
503 development in rice blast fungus (Deng *et al.* 2008; Kershaw and Talbot 2009).
504 These results together suggested that PoElp3 is required for the development,
505 pathogenicity and autophagy by regulating the translational efficiency of
506 proteins involved in diverse pathways.

507 Both sphingolipid and ergosterol are important component of plasma
508 membrane, and are involved in membrane trafficking (Hurst and Fratti 2020).
509 Recent study in MoErg4 revealed a role in the proper localization of the
510 *t*-soluble N-ethylmaleimide-sensitive factor attachment protein receptor
511 (SNARE) protein MoSso1 and subsequently the secretion of cytoplasmic
512 effector proteins in the rice blast fungus (Guo *et al.* 2023). Except for the
513 involvement in autophagy, a common function in different organisms (Li *et al.*
514 2014; Liu *et al.* 2019), sphingolipid is also required for fungal growth

515 (Ramamoorthy *et al.* 2009; Oura and Kajiwara 2010), and host - pathogen
516 interaction (Ramamoorthy *et al.* 2009; Singh *et al.* 2012; Wang *et al.* 2021). In
517 this study, functional classification revealed that some of the Erps were
518 involved in sphingolipid metabolism. And detailed analysis suggested that
519 PoElp3 is required for the translational efficiency of PoErp9, a sphingolipid
520 C9-methyltransferase, and therefore maintains the proper metabolism of
521 sphigolipid and the related cellular processes, including the asexual
522 development, pathogenicity and TOR-related autophage homeostasis.
523 However, how the PoErp9 act in these processed, particularly the
524 pathogenicity, in the blast fungus remains to be explored.
525 In conclusion, our results demonstrated that PoElp3 was involved in the
526 asexual development, pathogenicity, and autophagy, by regulating the
527 tRNA-mediated protein integrity.
528

529 **Acknowledgments**

530 This work was supported by National Natural Science Foundation of China to
531 H.Z (32172365) and Z.W (32272513), Central Guidance on Local Science and
532 Technology Development Fund of Fujian Province (2022L3088), and the
533 Innovative Research Funding of Fujian Agriculture and Forestry University,
534 China, to H.Z (CXZX2020153D).
535

536 **Competing interests**

537 The authors declare that they have no competing interests.

538

539 **Authors' contributions**

540 Z.W, G.L and H.Z conceived and designed the study. T.S, X.W and X.L
541 performed data analysis. Y.H.L, Y.Y.L, J.H, H.B, J.H, Z.Z, and T.W performed
542 the experiments. G.L, H.Z and Z.W wrote and revised the manuscript; GL, Z.W

543 and D.Z contributed to improvement of the manuscript. All authors read and
544 approved the final manuscript.
545

546 ## References

547 Abbassi NE, Biela A, Glatt S and Lin TY. 2020. How Elongator Acetylates tRNA Bases. *Int J Mol Sci,* **21,**

548 Anjago WM, Biregeya J, Shi M, Chen Y, Wang Y, Wang Z, Hong Y and Chen M. 2022. The calcium
549 chloride responsive type 2C protein phosphatases play synergistic roles in regulating MAPK
550 pathways in *Magnaporthe oryzae*. *J Fungi (Basel),* **8,**

551 Aron O, Otieno FJ, Tijjani I, Yang Z, Xu H, Weng S, Guo J, Lu S, Wang Z and Tang W. 2022. De novo
552 purine nucleotide biosynthesis mediated by MoAde4 is required for conidiation, host
553 colonization and pathogenicity in *Magnaporthe oryzae*. *Appl Microbiol Biotechnol,* **106,**
554 5587-5602.

555 Bauer F, Matsuyama A, Candiracci J, Dieu M, Scheliga J, Wolf DA, Yoshida M and Hermand D. 2012.
556 Translational control of cell division by Elongator. *Cell Rep,* **1,** 424-433.

557 Bhadauria V, Banniza S, Vandenberg A, Selvaraj G and Wei Y. 2012a. Alanine: Glyoxylate
558 aminotransferase 1 is required for mobilization and utilization of triglycerides during infection
559 process of the rice blast pathogen, *Magnaporthe oryzae*. *Plant Signal Behav,* **7,** 1206-1208.

560 Bhadauria V, Banniza S, Vandenberg A, Selvaraj G and Wei Y. 2012b. Peroxisomal alanine: glyoxylate
561 aminotransferase AGT1 is indispensable for appressorium function of the rice blast pathogen,
562 *Magnaporthe oryzae*. *PLoS One,* **7,** e36266.

563 Cai Q, Wang J, Xie J, Jiang D and Keyhani NO. 2022. The Elongator subunit Elp3 regulates development,
564 stress tolerance, cell cycle, and virulence in the entomopathogenic fungus *Beauveria*
565 *bassiana*. *J Fungi (Basel),* **8,**

566 Candiracci J, Migeot V, Chionh YH, Bauer F, Brochier T, Russell B, Shiozaki K, Dedon P and Hermand D.
567 2019. Reciprocal regulation of TORC signaling and tRNA modifications by Elongator enforces
568 nutrient-dependent cell fate. *Sci Adv,* **5,** eaav0184.

569 Cheng J, Yin Z, Zhang Z and Liang Y. 2018. Functional analysis of MoSnf7 in *Magnaporthe oryzae*.
570 *Fungal Genet Biol,* **121,** 29-45.

571 Creppe C, Malinouskaya L, Volvert ML, Gillard M, Close P, Malaise O, Laguesse S, Cornez I, Rahmouni S,
572 Ormenese S, Belachew S, Malgrange B, Chapelle JP, Siebenlist U, Moonen G, Chariot A and
573 Nguyen L. 2009. Elongator controls the migration and differentiation of cortical neurons
574 through acetylation of alpha-tubulin. *Cell,* **136,** 551-564.

575 Dauden MI, Jaciuk M, Weis F, Lin TY, Kleindienst C, Abbassi NEH, Khatter H, Krutyhołowa R, Breunig KD,
576 Kosinski J, Müller CW and Glatt S. 2019. Molecular basis of tRNA recognition by the Elongator
577 complex. *Sci Adv,* **5,** eaaw2326.
578 Dean RA, Talbot NJ, Ebbole DJ, Farman ML, Mitchell TK, Orbach MJ, Thon M, Kulkarni R, Xu JR, Pan H,
579 Read ND, Lee YH, Carbone I, Brown D, Oh YY, Donofrio N, Jeong JS, Soanes DM, Djonovic S,
580 Kolomiets E, Rehmeyer C, Li W, Harding M, Kim S, Lebrun MH, Bohnert H, Coughlan S, Butler J,
581 Calvo S, Ma LJ, Nicol R, Purcell S, Nusbaum C, Galagan JE and Birren BW. 2005. The genome
582 sequence of the rice blast fungus *Magnaporthe grisea*. *Nature,* **434,** 980-986.
583 Deng YZ, Ramos-Pamplona M and Naqvi NI. 2008. Methods for functional analysis of macroautophagy
584 in filamentous fungi. *Methods Enzymol,* **451,** 295-310.
585 Dewez M, Bauer F, Dieu M, Raes M, Vandenhaute J and Hermand D. 2008. The conserved Wobble
586 uridine tRNA thiolase Ctu1-Ctu2 is required to maintain genome integrity. *Proc Natl Acad Sci*
587 *U S A,* **105,** 5459-5464.
588 Esberg A, Huang B, Johansson MJ and Byström AS. 2006. Elevated levels of two tRNA species bypass
589 the requirement for elongator complex in transcription and exocytosis. *Mol Cell,* **24,** 139-148.
590 Giraldo MC, Dagdas YF, Gupta YK, Mentlak TA, Yi M, Martinez-Rocha AL, Saitoh H, Terauchi R, Talbot NJ
591 and Valent B. 2013. Two distinct secretion systems facilitate tissue invasion by the rice blast
592 fungus *Magnaporthe oryzae*. *Nat Commun,* **4,** 1996.
593 Goffena J, Lefcort F, Zhang Y, Lehrmann E, Chaverra M, Felig J, Walters J, Buksch R, Becker KG and
594 George L. 2018. Elongator and codon bias regulate protein levels in mammalian peripheral
595 neurons. *Nat Commun,* **9,** 889.
596 Guo Z, Liu X, Wang N, Mo P, Shen J, Liu M, Zhang H, Wang P and Zhang Z. 2023. Membrane
597 component ergosterol builds a platform for promoting effector secretion and virulence in
598 *Magnaporthe oryzae*. *New Phytol,* **237,** 930-943.
599 He M, Xu Y, Chen J, Luo Y, Lv Y, Su J, Kershaw MJ, Li W, Wang J, Yin J, Zhu X, Liu X, Chern M, Ma B, Wang
600 J, Qin P, Chen W, Wang Y, Wang W, Ren Z, Wu X, Li P, Li S, Peng Y, Lin F, Talbot NJ and Chen X.
601 2018. MoSnt2-dependent deacetylation of histone H3 mediates MoTor-dependent
602 autophagy and plant infection by the rice blast fungus *Magnaporthe oryzae*. *Autophagy,* **14,**
603 1543-1561.
604 Holley RW, Apgar J, Everett GA, Madison JT, Marquisee M, Merrill SH, Penswick JR and Zamir A. 1965.
605 STRUCTURE OF A RIBONUCLEIC ACID. *Science,* **147,** 1462-1465.
606 Hurst LR and Fratti RA. 2020. Lipid rafts, sphingolipids, and ergosterol in yeast vacuole fusion and
607 maturation. *Front Cell Dev Biol,* **8,** 539.

608 Jaciuk M, Scherf D, Kaszuba K, Gaik M, Rau A, Kościelniak A, Krutyhołowa R, Rawski M, Indyka P,
609 Graziadei A, Chramiec-Głąbik A, Biela A, Dobosz D, Lin TY, Abbassi NE, Hammermeister A,
610 Rappsilber J, Kosinski J, Schaffrath R and Glatt S. 2023. Cryo-EM structure of the fully
611 assembled Elongator complex. *Nucleic Acids Res,* **51,** 2011-2032.

612 Johansson MJ, Esberg A, Huang B, Björk GR and Byström AS. 2008. Eukaryotic wobble uridine
613 modifications promote a functionally redundant decoding system. *Mol Cell Biol,* **28,**
614 3301-3312.

615 Karimi Aghcheh R, Druzhinina IS and Kubicek CP. 2013. The putative protein methyltransferase LAE1 of
616 Trichoderma atroviride is a key regulator of asexual development and mycoparasitism. *PLoS*
617 *One,* **8,** e67144.

618 Kershaw MJ and Talbot NJ. 2009. Genome-wide functional analysis reveals that infection-associated
619 fungal autophagy is necessary for rice blast disease. *Proc Natl Acad Sci U S A,* **106,**
620 15967-15972.

621 Laguesse S, Close P, Van Hees L, Chariot A, Malgrange B and Nguyen L. 2017. Loss of Elp3 impairs the
622 acetylation and distribution of connexin-43 in the developing cerebral cortex. *Front Cell*
623 *Neurosci,* **11,** 122.

624 Lee Y, Min K, Son H, Park AR, Kim JC, Choi GJ and Lee YW. 2014. ELP3 is involved in sexual and asexual
625 development, virulence, and the oxidative stress response in *Fusarium graminearum*. *Mol*
626 *Plant Microbe Interact,* **27,** 1344-1355.

627 Leidel S, Pedrioli PG, Bucher T, Brost R, Costanzo M, Schmidt A, Aebersold R, Boone C, Hofmann K and
628 Peter M. 2009. Ubiquitin-related modifier Urm1 acts as a sulphur carrier in thiolation of
629 eukaryotic transfer RNA. *Nature,* **458,** 228-232.

630 Li B and Dewey CN. 2011. RSEM: accurate transcript quantification from RNA-Seq data with or without
631 a reference genome. *BMC Bioinformatics,* **12,** 323.

632 Li G, Dulal N, Gong Z and Wilson RA. 2023. Unconventional secretion of *Magnaporthe oryzae* effectors
633 in rice cells is regulated by tRNA modification and codon usage control. *Nat Microbiol,* **8,**
634 1706-1716.

635 Li Y, Li S, Qin X, Hou W, Dong H, Yao L and Xiong L. 2014. The pleiotropic roles of sphingolipid signaling
636 in autophagy. *Cell Death Dis,* **5,** e1245.

637 Lin TY, Abbassi NEH, Zakrzewski K, Chramiec-Głąbik A, Jemioła-Rzemińska M, Różycki J and Glatt S.
638 2019. The Elongator subunit Elp3 is a non-canonical tRNA acetyltransferase. *Nat Commun,* **10,**
639 625.

640 Liu XH, Liang S, Wei YY, Zhu XM, Li L, Liu PP, Zheng QX, Zhou HN, Zhang Y, Mao LJ, Fernandes CM, Del

641 Poeta M, Naqvi NI and Lin FC. 2019. Metabolomics analysis identifies sphingolipids as key
642 signaling moieties in appressorium morphogenesis and function in *Magnaporthe oryzae*.
643 *mBio,* **10,**

644 Liu XH, Lu JP, Zhang L, Dong B, Min H and Lin FC. 2007. Involvement of a *Magnaporthe grisea*
645 serine/threonine kinase gene, MgATG1, in appressorium turgor and pathogenesis. *Eukaryot*
646 *Cell,* **6,** 997-1005.

647 Ma X, Liu C and Cao X. 2021. Plant transfer RNA-derived fragments: Biogenesis and functions. *J Integr*
648 *Plant Biol,* **63,** 1399-1409.

649 Miśkiewicz K, Jose LE, Bento-Abreu A, Fislage M, Taes I, Kasprowicz J, Swerts J, Sigrist S, Versées W,
650 Robberecht W and Verstreken P. 2011. ELP3 controls active zone morphology by acetylating
651 the ELKS family member Bruchpilot. *Neuron,* **72,** 776-788.

652 Moreau K, Ravikumar B, Puri C and Rubinsztein DC. 2012. Arf6 promotes autophagosome formation
653 via effects on phosphatidylinositol 4,5-bisphosphate and phospholipase D. *J Cell Biol,* **196,**
654 483-496.

655 Nedialkova DD and Leidel SA. 2015. Optimization of codon translation rates via tRNA modifications
656 maintains proteome integrity. *Cell,* **161,** 1606-1618.

657 Otero G, Fellows J, Li Y, de Bizemont T, Dirac AM, Gustafsson CM, Erdjument-Bromage H, Tempst P and
658 Svejstrup JQ. 1999. Elongator, a multisubunit component of a novel RNA polymerase II
659 holoenzyme for transcriptional elongation. *Mol Cell,* **3,** 109-118.

660 Oura T and Kajiwara S. 2010. *Candida albicans* sphingolipid C9-methyltransferase is involved in hyphal
661 elongation. *Microbiology (Reading),* **156,** 1234-1243.

662 Planelles-Herrero VJ, Bittleston A, Seum C, Daeden A, Gaitan MG and Derivery E. 2022. Elongator
663 stabilizes microtubules to control central spindle asymmetry and polarized trafficking of cell
664 fate determinants. *Nat Cell Biol,* **24,** 1606-1616.

665 Ramamoorthy V, Cahoon EB, Thokala M, Kaur J, Li J and Shah DM. 2009. Sphingolipid C-9
666 methyltransferases are important for growth and virulence but not for sensitivity to
667 antifungal plant defensins in Fusarium graminearum. *Eukaryot Cell,* **8,** 217-229.

668 Selvadurai K, Wang P, Seimetz J and Huang RH. 2014. Archaeal Elp3 catalyzes tRNA wobble uridine
669 modification at C5 via a radical mechanism. *Nat Chem Biol,* **10,** 810-812.

670 Singh A, Wang H, Silva LC, Na C, Prieto M, Futerman AH, Luberto C and Del Poeta M. 2012.
671 Methylation of glycosylated sphingolipid modulates membrane lipid topography and
672 pathogenicity of *Cryptococcus neoformans*. *Cell Microbiol,* **14,** 500-516.

673 Sokołowski M, Klassen R, Bruch A, Schaffrath R and Glatt S. 2018. Cooperativity between different
674 tRNA modifications and their modification pathways. *Biochim Biophys Acta Gene Regul Mech,*
675 **1861,** 409-418.

676 Sun G, Elowsky C, Li G and Wilson RA. 2018. TOR-autophagy branch signaling via Imp1 dictates
677 plant-microbe biotrophic interface longevity. *PLoS Genet,* **14,** e1007814.

678 Sweigard JA, Carroll AM, Farrall L, Chumley FG and Valent B. 1998. *Magnaporthe grisea* pathogenicity
679 genes obtained through insertional mutagenesis. *Mol Plant Microbe Interact,* **11,** 404-412.

680 Tükenmez H, Xu H, Esberg A and Byström AS. 2015. The role of wobble uridine modifications in +1
681 translational frameshifting in eukaryotes. *Nucleic Acids Res,* **43,** 9489-9499.

682 Valent B, Farrall L and Chumley FG. 1991. *Magnaporthe grisea* genes for pathogenicity and virulence
683 identified through a series of backcrosses. *Genetics,* **127,** 87-101.

684 Wang J, Chen Y-L, Li Y-K, Chen D-K, He J-F and Yao N. 2021. Functions of sphingolipids in pathogenesis
685 during host–pathogen interactions. **12,**

686 Wilson RA and Talbot NJ. 2009. Under pressure: investigating the biology of plant infection by
687 *Magnaporthe oryzae*. *Nat Rev Microbiol,* **7,** 185-195.

688 Winkler GS, Kristjuhan A, Erdjument-Bromage H, Tempst P and Svejstrup JQ. 2002. Elongator is a
689 histone H3 and H4 acetyltransferase important for normal histone acetylation levels *in vivo*.
690 *Proc Natl Acad Sci U S A,* **99,** 3517-3522.

691 Wittschieben BO, Fellows J, Du W, Stillman DJ and Svejstrup JQ. 2000. Overlapping roles for the
692 histone acetyltransferase activities of SAGA and elongator *in vivo*. *Embo j,* **19,** 3060-3068.

693 Xie J, Tang W, Lu G, Hong Y, Zhong Z, Wang Z and Zheng H. 2023. Histone H3K27me3 methylation
694 regulates the expression of secreted proteins distributed at fast-evolving regions through
695 transcriptional repression of transposable elements. *Journal of Integrative Agriculture,*

696 Yang F and Naqvi NI. 2014. Sulfonylurea resistance reconstitution as a novel strategy for ILV2-specific
697 integration in *Magnaporthe oryzae*. *Fungal Genetics and Biology,* **68,** 71-76.

698 Yin Z, Chen C, Yang J, Feng W, Liu X, Zuo R, Wang J, Yang L, Zhong K, Gao C, Zhang H, Zheng X, Wang P
699 and Zhang Z. 2019. Histone acetyltransferase MoHat1 acetylates autophagy-related proteins
700 MoAtg3 and MoAtg9 to orchestrate functional appressorium formation and pathogenicity in
701 *Magnaporthe oryzae*. *Autophagy,* **15,** 1234-1257.

702 Zhang L, Chen S, Qi M, Cao X, Liang N, Li Q, Tang W, Lu G, Zhou J, Yu W, Wang Z and Zheng H. 2021.
703 The putative elongator complex protein Elp3 is involved in asexual development and

704 pathogenicity by regulating autophagy in the rice blast fungus. *Journal of Integrative*
705 *Agriculture,* **20,** 2944-2956.

706 Zhang Y, Wang Y, Fan J, Zhu G and Lu L. 2022. *Aspergillus fumigatus* Elongator complex subunit 3
707 affects hyphal growth, adhesion and virulence through wobble uridine tRNA modification.
708 *PLoS Pathog,* **18,** e1010976.

709 Zhao W, Li C, Liang J and Sun S. 2014. The *Aspergillus fumigatus* β-1,3-glucanosyltransferase Gel7 plays
710 a compensatory role in maintaining cell wall integrity under stress conditions. *Glycobiology,*
711 **24,** 418-427.

712 Zheng H, Guo Z, Xi Y, Yuan M, Lin Y, Wu C, Abubakar YS, Dou X, Li G, Wang Z, Zheng W and Zhou J. 2017.
713 Sorting nexin (MoVps17) is required for fungal development and plant infection by regulating
714 endosome dynamics in the rice blast fungus. *Environ Microbiol,* **19,** 4301-4317.

715 Zheng W, Chen J, Liu W, Zheng S, Zhou J, Lu G and Wang Z. 2007. A Rho3 homolog is essential for
716 appressorium development and pathogenicity of *Magnaporthe grisea*. *Eukaryot Cell,* **6,**
717 2240-2250.

718 Zhong Z, Lin L, Chen M, Lin L, Chen X, Lin Y, Chen X, Wang Z, Norvienyeku J and Zheng H. 2019.
719 Expression Divergence as an evolutionary alternative mechanism adopted by two rice
720 subspecies against rice blast infection. *Rice (N Y),* **12,** 12.

721 Zhu S, Yan Y, Qu Y, Wang J, Feng X, Liu X, Lin F and Lu J. 2021. Role refinement of melanin synthesis
722 genes by gene knockout reveals their functional diversity in *Pyricularia oryzae strains*.
723 *Microbiol Res,* **242,** 126620.

724 Zhu X, Zhou T, Chen L, Zheng S, Chen S, Zhang D, Li G and Wang Z. 2016. Arf6 controls endocytosis and
725 polarity during asexual development of *Magnaporthe oryzae*. *FEMS Microbiol Lett,* **363,**

726

727 **Figure legends**

728 **Fig. 1** Overexpression of *tK*(*UUU*) or *tQ*(*UUG*) could partially rescue the
729 defects in Δ*Poelp3* strain. A, the indicated strains grown on CM, MM and MM
730 supplemented with 1 μg/uL rapamycin (MM+Rap). B, colony diameter of
731 indicated strains grown on CM. C, the inhibition rate of indicated strains upon
732 the treatment of 1 μg/uL rapamycin. The letters indicate statistically significant
733 differences ($p<0.01$). D, leaves of rice cultivar TP309 were sprayed with
734 conidial suspensions (5×10^4conidia mL^{-1}) of strains indicated. E, quantification
735 of different lesion types. Data were shown as the mean±SE (n=3).

736 **Fig. 2** The differentially accumulated proteins (DAPs) between Δ*Poelp3* and
737 Guy11 strains. A, quantitative identification of proteins upregulated and
738 downregulated in Δ*Poelp3* strain though TMT. B, volcano plot showing the fold
739 change of the differentially accumulated proteins. C, cluster analysis of the
740 DAPs.
741 **Fig. 3** Functional classification of the DAPs. A, the four Q Categories of the
742 DAPs. B, classification of DAPs according to the KEGG pathway. C,
743 classification of DAPs according to protein domain.
744 **Fig. 4** Comparative transcriptional analysis between wild type and Δ*Poelp3*
745 strains. A, differentially expressed genes between wild type and Δ*Poelp3*
746 strains. B, comparative analysis of the transcription level of DAPs
747 down-regulated in Δ*Poelp3* strain.
748 Fig. 5 The abundance of PoErp9 was reduced in the Δ*Poelp3* strain. A,
749 strategy for the *in situ* fusion of *PoERP9-GFP* into the sulfonylurea-resistant
750 allele of the *ILV2* gene. B, the relative abundance of PoErp9-GFP
751 [GFP/(GFP+GFP-PoAtg8)] in wild type (Guy11) and Δ*Poelp3* strains. The
752 numbers indicated different individual transfromants. C, relative transcription
753 level of *PoERP9* in wild type (Guy11) and Δ*Poelp3* strains based on qRT-PCR.
754 Fig. 6 The Poerp9 strain was defective in asexual development and
755 pathogenicity. A and B, the colony morphology (A) and colony diameter (B) of
756 indicated strains on complete medium (CM) and minimal medium (MM) for 7
757 days. C, number of conidia harvested from a 7-cm rice bran plate at 3 days
758 after induction of conidiation. D, appressorial development of Ku80, ΔPoerp9
759 and ΔPoerp9c was observed using microscope at 4, 8 and 12 h after induction.
760 Data were shown as the mean±SE (n=3). The asterisks indicate statistically
761 significant differences (**, P<0.01; ***, P<0.001). E, leaves of rice cultivar NPB
762 were sprayed with conidial suspensions (5×104 conidia mL–1) of strains
763 indicated. E, quantification of different lesion types. Data were shown as the
764 mean±SE (n=3).
765 **Fig. 7** PoErp9 genetically interact with TOR-signaling to regulate vegetative

766 and invasive growth of rice blast fungus. A and C, colony morphology (A) and
767 inhibition rate of vegetative growth of indicated strains on minimal medium
768 (MM) treated with rapamycin (Rap). C and D, morphology (C) and types (D) of
769 invasive hyphae in *Ku80*, Δ*Poerp9* and Δ*Poerp9*c at 24 h post-inoculation (hpi).
770 Data were shown as the mean±SE (n=3).
771 **Table 1** Codon usage of lysine, glutamine and glutamic acid in the Erps.
772 **Table 2** The *ERPs* functionally studied in *P. oryzae*
773
774 **Supporting information**
775 **Appendix A.** Alignment of tRNAs from *Schizosaccharomyces pombe* (fission
776 yeast) and *P. oryzae*.
777 **Appendix B.** Primers used in this study.
778 **Appendix C.** Generation of Δ*Poerp9* mutant.
779 **Appendix D.** Proteins up-regulated in Δ*Poelp3* strain.
780 **Appendix E.** Proteins down-regulated in Δ*Poelp3* strain.
781 **Appendix F.** The transcription level of DAPs down-regulated in Δ*Poelp3* strain.
782 **Appendix G.** Comparative analysis of the transcription level of DAPs
783 up-regulated in Δ*Poelp3* strain.
784 **Appendix H.** Codons used in Erps.
785 **Appendix I.** Southern bloting assays for the *ILV2*-specific PoERP9-GFP
786 integration strains.
787 **Appendix J.** Ectopic expression of *PoERP9-GFP* could rescue the defect in
788 fungal growth of Δ*Poerp9* strain.
789

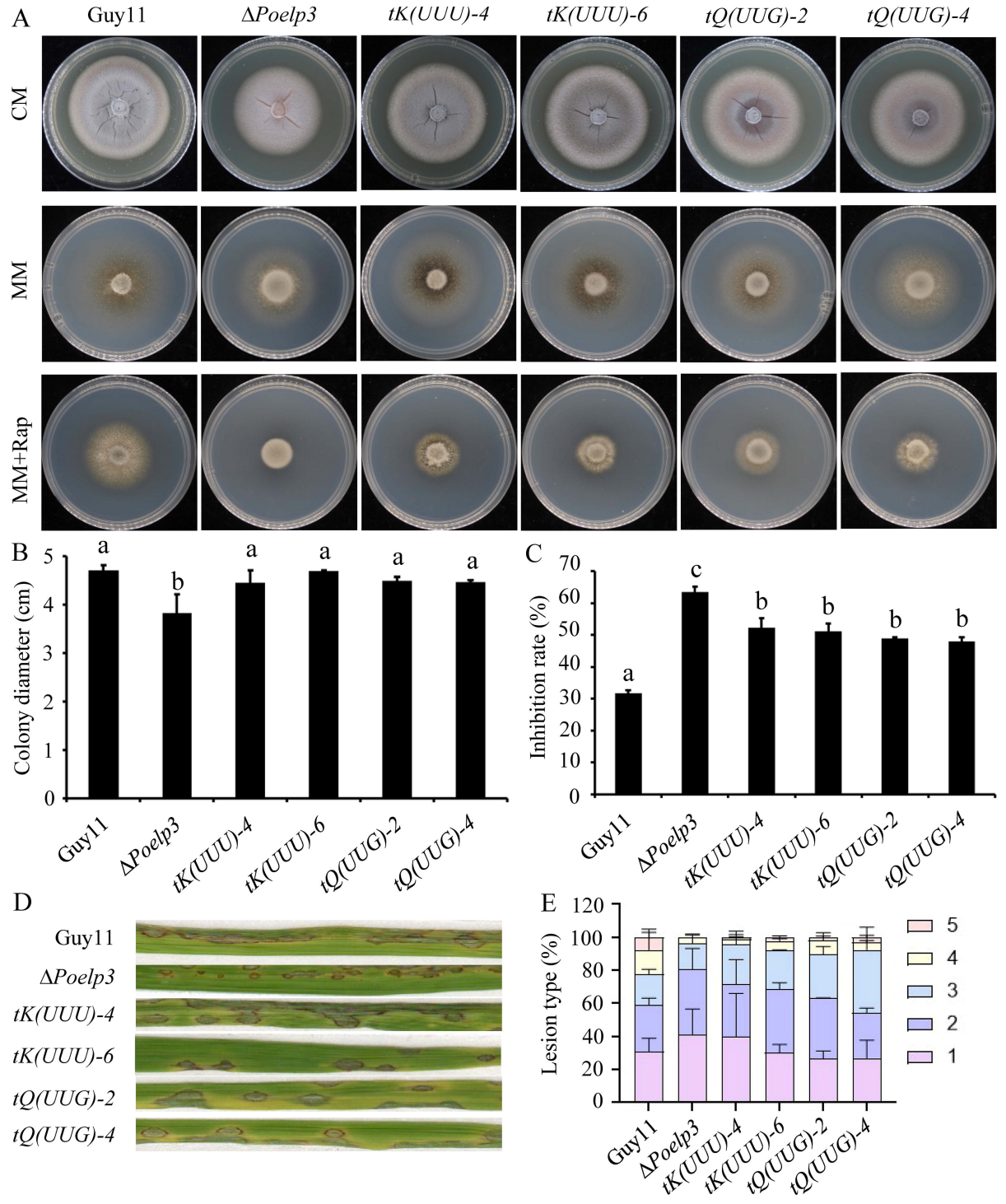
A
Guy11
ΔPoelp3
tK(UUU)-4
tK(UUU)-6
tQ(UUG)-2
tQ(UUG)-4
CM
MM
MM+Rap
B
Colony diameter (cm)
0
1
2
3
4
5
a
b
a
a
a
a
Guy11
ΔPoelp3
tK(UUU)-4
tK(UUU)-6
tQ(UUG)-2
tQ(UUG)-4
C
Inhibition rate (%)
0
10
20
30
40
50
60
70
a
c
b
b
b
b
Guy11
ΔPoelp3
tK(UUU)-4
tK(UUU)-6
tQ(UUG)-2
tQ(UUG)-4
D
Guy11
ΔPoelp3
tK(UUU)-4
tK(UUU)-6
tQ(UUG)-2
tQ(UUG)-4
E
Lesion type (%)
0
20
40
60
80
100
120
5
4
3
2
1
Guy11
ΔPoelp3
tK(UUU)-4
tK(UUU)-6
tQ(UUG)-2
tQ(UUG)-4

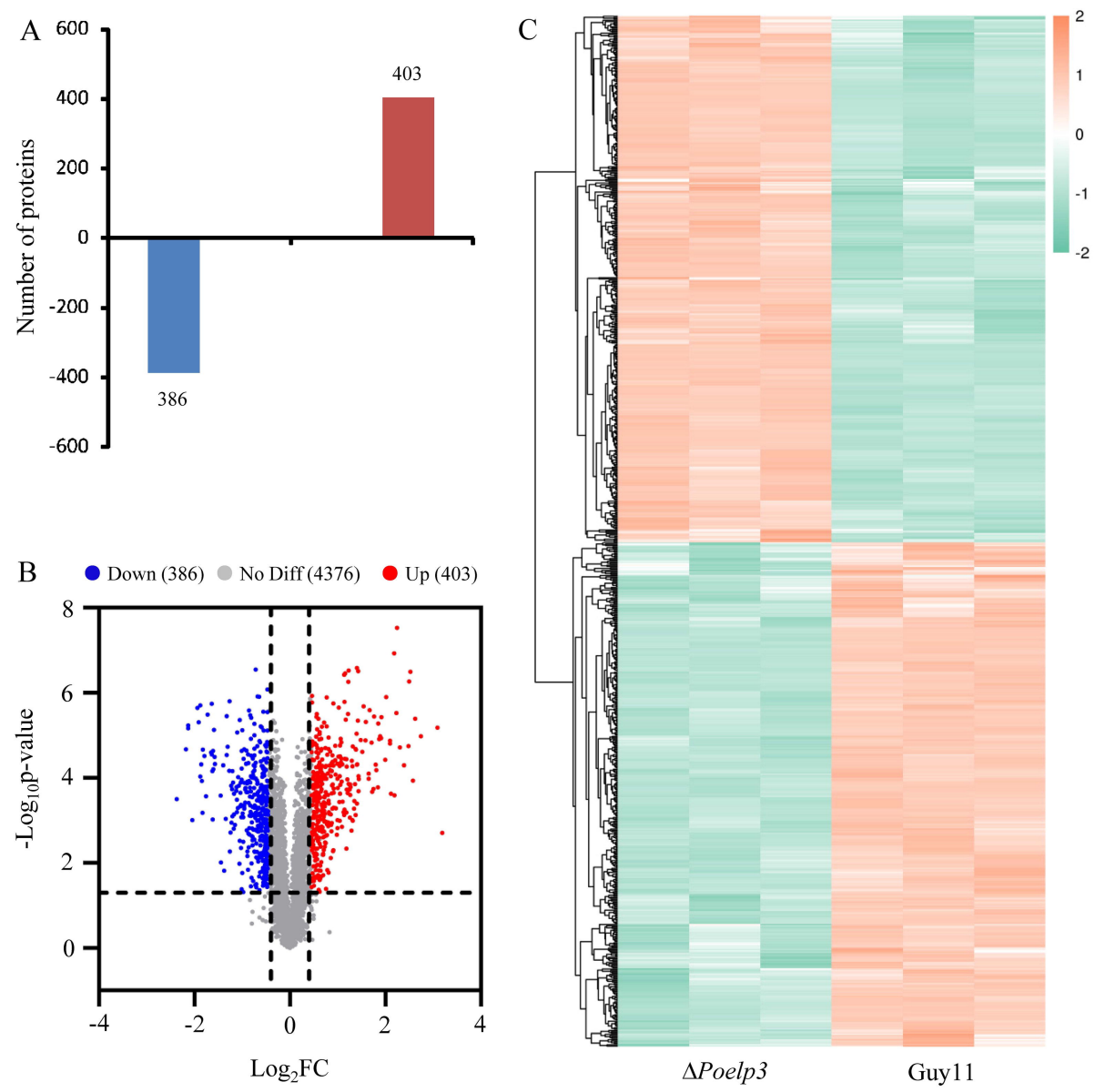
A
Number of proteins
600
400
200
0
-200
-400
-600
403
386
B
Down (386)
No Diff (4376)
Up (403)
-Log10p-value
8
6
4
2
0
-4
-2
0
2
4
Log2FC
C
2
1
0
-1
-2
ΔPoelp3
Guy11

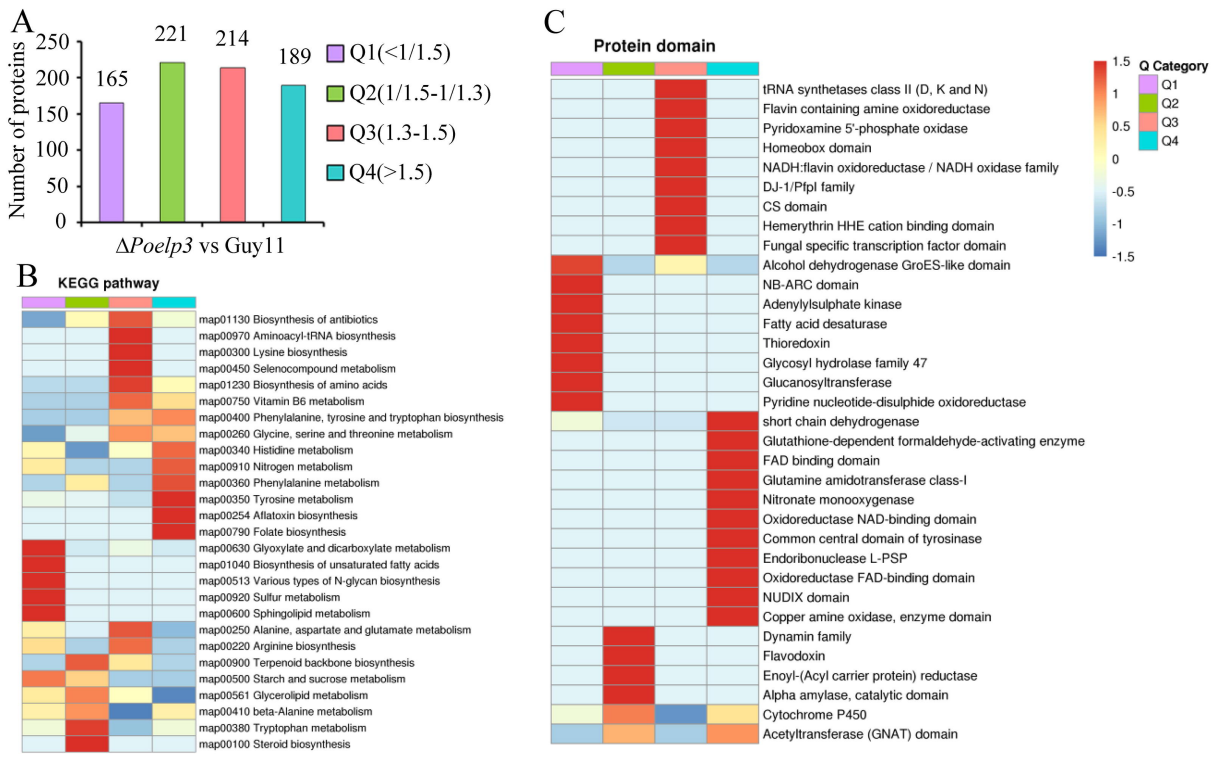
A
Number of proteins
250
200
150
100
50
0
165
221
214
189
Q1(<1/1.5)
Q2(1/1.5-1/1.3)
Q3(1.3-1.5)
Q4(>1.5)
ΔPoelp3 vs Guy11
B
KEGG pathway
map01130 Biosynthesis of antibiotics
map00970 Aminoacyl-tRNA biosynthesis
map00300 Lysine biosynthesis
map00450 Selenocompound metabolism
map01230 Biosynthesis of amino acids
map00750 Vitamin B6 metabolism
map00400 Phenylalanine, tyrosine and tryptophan biosynthesis
map00260 Glycine, serine and threonine metabolism
map00340 Histidine metabolism
map00910 Nitrogen metabolism
map00360 Phenylalanine metabolism
map00350 Tyrosine metabolism
map00254 Aflatoxin biosynthesis
map00790 Folate biosynthesis
map00630 Glyoxylate and dicarboxylate metabolism
map01040 Biosynthesis of unsaturated fatty acids
map00513 Various types of N-glycan biosynthesis
map00920 Sulfur metabolism
map00600 Sphingolipid metabolism
map00250 Alanine, aspartate and glutamate metabolism
map00220 Arginine biosynthesis
map00900 Terpenoid backbone biosynthesis
map00500 Starch and sucrose metabolism
map00561 Glycerolipid metabolism
map00410 beta-Alanine metabolism
map00380 Tryptophan metabolism
map00100 Steroid biosynthesis
C
Protein domain
tRNA synthetases class II (D, K and N)
Flavin containing amine oxidoreductase
Pyridoxamine 5'-phosphate oxidase
Homeobox domain
NADH:flavin oxidoreductase / NADH oxidase family
DJ-1/PfpI family
CS domain
Hemerythrin HHE cation binding domain
Fungal specific transcription factor domain
Alcohol dehydrogenase GroES-like domain
NB-ARC domain
Adenylylsulphate kinase
Fatty acid desaturase
Thioredoxin
Glycosyl hydrolase family 47
Glucanosyltransferase
Pyridine nucleotide-disulphide oxidoreductase
short chain dehydrogenase
Glutathione-dependent formaldehyde-activating enzyme
FAD binding domain
Glutamine amidotransferase class-I
Nitronate monooxygenase
Oxidoreductase NAD-binding domain
Common central domain of tyrosinase
Endoribonuclease L-PSP
Oxidoreductase FAD-binding domain
NUDIX domain
Copper amine oxidase, enzyme domain
Dynamin family
Flavodoxin
Enoyl-(Acyl carrier protein) reductase
Alpha amylase, catalytic domain
Cytochrome P450
Acetyltransferase (GNAT) domain
1.5
1
0.5
0
-0.5
-1
-1.5
Q Category
Q1
Q2
Q3
Q4

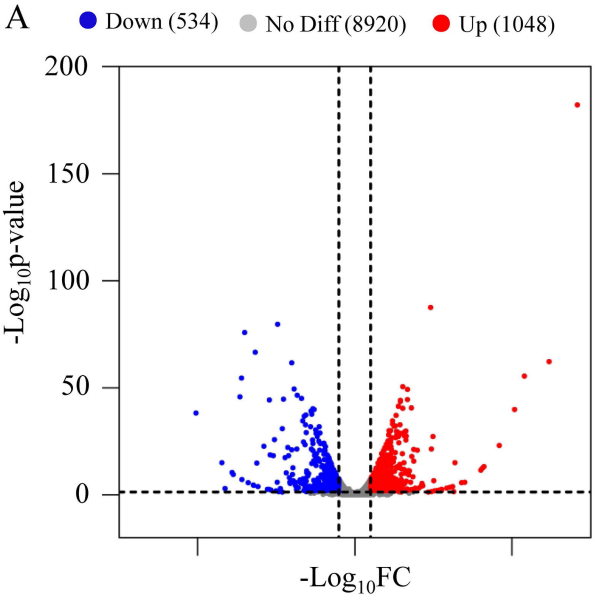
A
Down (534)
No Diff (8920)
Up (1048)
200
150
100
50
0
-Log10p-value
-Log10FC

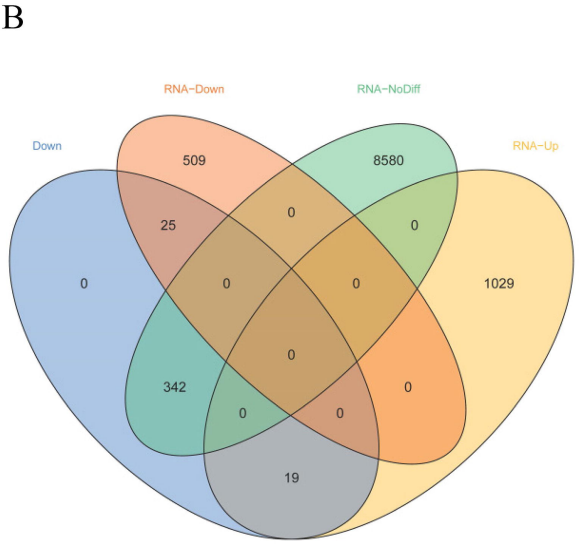
B
Down
RNA-Down
RNA-NoDiff
RNA-Up
0
509
8580
1029
25
0
0
0
0
0
342
0
0
0
19

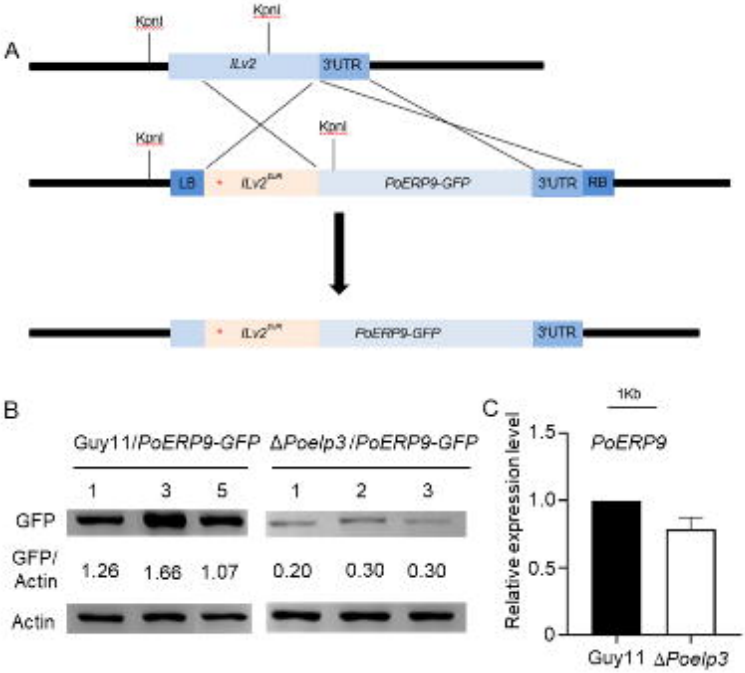
A
KpnI
KpnI
iLv2
3'UTR
KpnI
KpnI
LB
iLv2
PoERP9-GFP
3'UTR
RB
iLv2
PoERP9-GFP
3'UTR
B
Guy11/PoERP9-GFP
ΔPoelp3/PoERP9-GFP
1
3
5
1
2
3
GFP
GFP/
Actin
1.26
1.66
1.07
0.20
0.30
0.30
Actin
C
1Kb
PoERP9
Relative expression level
1.5
1.0
0.5
0
Guy11
ΔPoelp3

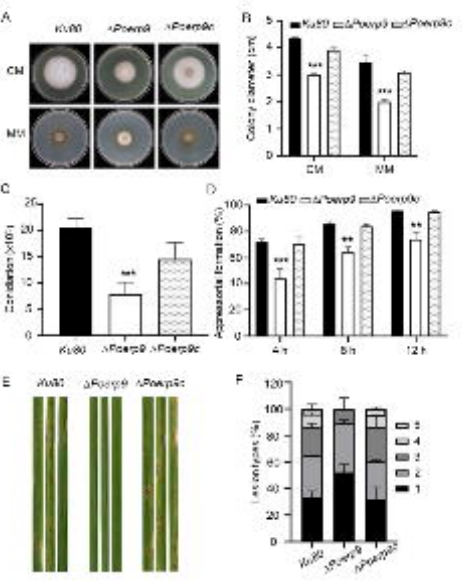
A
Ku80
ΔPoerp9
ΔPoerp9c
CM
MM
B
Ku80
ΔPoerp9
ΔPoerp9c
Colony diameter (cm)
CM
MM
C
Conidiation (×10⁶)
Ku80
ΔPoerp9
ΔPoerp9c
D
Ku80
ΔPoerp9
ΔPoerp9c
Appressoria formation (%)
4 h
8 h
12 h
E
Ku80
ΔPoerp9
ΔPoerp9c
F
Lesion type (%)
Ku80
ΔPoerp9
ΔPoerp9c

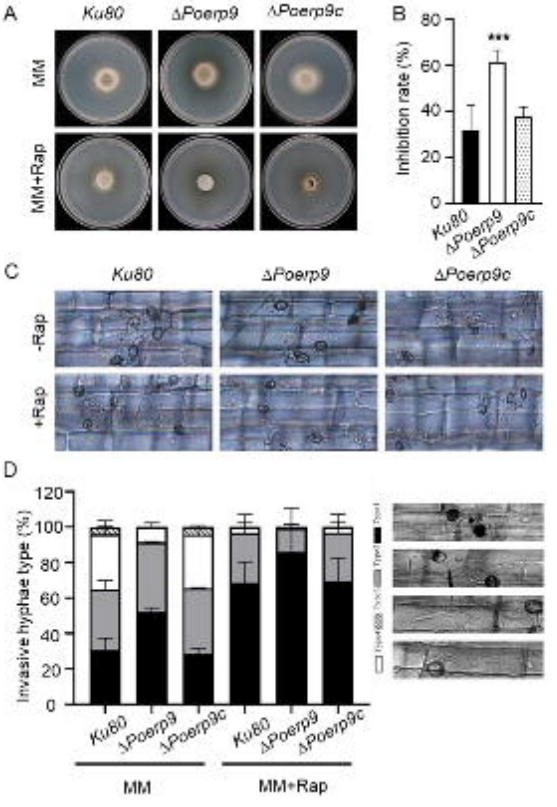
A
Ku80
ΔPoerp9
ΔPoerp9c
MM
MM+Rap
B
Inhibition rate (%)
80
60
40
20
0
***
Ku80
ΔPoerp9
ΔPoerp9c
C
Ku80
ΔPoerp9
ΔPoerp9c
-Rap
+Rap
D
Invasive hyphae type (%)
120
100
80
60
40
20
0
Ku80
ΔPoerp9
ΔPoerp9c
Ku80
ΔPoerp9
ΔPoerp9c
MM
MM+Rap